Throughput-Delay Tradeoff Management for Partially Connected Networks via Lyapunov Drift Optimization

Throughput-Delay Tradeoff Management for Partially Connected Networks via Lyapunov Drift Optimization

Shaohua Cui, Lichao Wang, Yongjie Xue, Kaidi Yang, *Member, IEEE*, and Kun Gao, *Member, IEEE*

***Abstract*—Network-level traffic signal control is an effective way to increase throughput and reduce congestion. The max-pressure algorithm, known for maximizing network throughput, has been widely studied. However, it requires accurate queue length and turn ratio measurements, and its theoretical guarantee is limited to feasible demand (i.e., demand within the capacity region) under the assumption of infinite queue capacity. To overcome these limitations, this study proposes a distributed joint admission and signal control algorithm for finite-capacity networks with both connected and regular vehicles. By using feedback from connected vehicles, the algorithm estimates queue lengths and turn ratios, reducing reliance on precise measurements. It also adaptively adjusts input flow rates to prevent oversaturation and ensure demand feasibility, even under high-demand conditions, while optimizing signal phases to ensure analytic performance. Using a Lyapunov drift optimization approach, we analytically prove a $[O(1/V), O(V)]$ tradeoff between throughput and delay and establish degradation bounds that quantify the impact of queue length estimation errors on network performance. Simulations in a network with 256 origin-destination pairs show up to a 16.3% increase in throughput and reduced delays, especially in high-demand settings. The method also demonstrates strong resilience to sudden demand changes and incidents, ensuring quick recovery.**

***Index Terms*—Adaptive signal control, admission control, max pressure, mixed traffic.**

I. Introduction

TRAFFIC congestion is a significant issue in major cities worldwide, with substantial economic and environmental impacts [1]. In contrast to control strategies designed for isolated intersections [2], [3], network-level signal control has emerged as an effective method of improving network capacity and alleviating congestion without significantly affecting traveler route choices [4], [5]. Current network-level traffic signal control algorithms adopt predominantly centralized control methods, including optimization-based approaches [6], [7] and data-driven approaches [8], [9], [10]. However, these centralized methods face scalability challenges. As urban networks expand, maintaining solution efficiency becomes difficult and real-time signal phase updates are hard to guarantee, which limits their applicability to large-scale networks. These scalability limitations have motivated growing research into distributed traffic signal control, including the asymmetric two-bin signal control [11], coordinated model predictive control [12], [13], asymmetric advantage actor-critic (Asym-A2C) algorithm [14], linear quadratic regulator [15], adaptive and cooperative traffic light agent model (ACTAM) [16], and max pressure (MP) signal control (also known as back pressure) [17], [18], which have recently gained prominence.

Among these distributed signal control approaches, MP signal control has garnered significant attention. Originally derived from communications and introduced to traffic signal control by [19] and [20], MP signal control relies solely on queue length information from adjacent links and average turn ratios for real-time signal phase optimization. MP signal control, assuming infinite queue capacity, is analytically proven to ensure network queue stability (i.e., maintaining bounded average queue lengths at intersections) when demand does not exceed network capacity [21]. The queue-stable network means that all incoming demand can be effectively serviced, which has led to numerous studies claiming that it maximizes network throughput. MP signal control's analytical provability, suitability for distributed implementation, and independence from pre-estimated demand arrival rates have led to its recent expansion in various directions. These include considering cyclical signal phases [22], [23], addressing waiting delay [24], [25], reducing phase switching losses [26], incorporating dynamic lane reversal [27], integrating transit lines [28], integrating dedicated lanes for autonomous vehicles [29], accommodating pedestrians [30], and accounting for how vehicles are spatially distributed along links [18].

However, these enhancements typically depend on accurate average turn ratio estimations, often requiring extensive historical data. Lioris et al. [31] and Gregoire et al. [32] developed algorithms for estimating turn ratios. Le et al. [33] optimized these ratios, while Zaidi et al. [34] integrated vehicle

Received 21 March 2025; revised 21 November 2025; accepted 22 January 2026. Date of publication 2 February 2026; date of current version 2 June 2026. This work was supported by the Area of Advance Transport at Chalmers University of Technology and VINNOVA under Grant 2024-00810. The Associate Editor for this article was W.-H. Lin. *(Corresponding author: Kun Gao.)*

Shaohua Cui and Kun Gao are with the Department of Architecture and Civil Engineering, Chalmers University of Technology, 412 96 Gothenburg, Sweden (e-mail: shaohuac@chalmers.se; gkun@chalmers.se).

Lichao Wang is with the College of Air Traffic Management, Civil Aviation University of China, Tianjin 300300, China (e-mail: lcwang@cauc.edu.cn).

Yongjie Xue is with the School of Transportation Science and Engineering, Beihang University, Beijing 100191, China (e-mail: xueyongjie@buaa.edu.cn).

Kaidi Yang is with the Department of Civil and Environmental Engineering, National University of Singapore, Singapore 119077 (e-mail: kaidi.yang@nus.edu.sg).

This article has supplementary downloadable material available at https://doi.org/10.1109/TITS.2026.3659040, provided by the authors.

Digital Object Identifier 10.1109/TITS.2026.3659040

path optimization into MP signal control to reduce reliance on accurate turn ratio information. These studies, however, have relied on precise queue length information feasible only in fully connected environments. The complete transition to fully connected networks remains a distant goal [35], [36], [37]. In the foreseeable future, road networks are poised to become heterogeneous compositions of connected vehicles (CVs) and regular vehicles (RVs), creating challenging mixed traffic scenarios [38]. Although Li et al. [39] developed algorithms for queue length estimations, they have neither analytically examined how estimation errors in queue lengths affect network queue stability nor analyzed the consequent degradation in average delay and network throughput.

In addition, most existing studies assume infinite queue capacity in networks when proving network stability. Numerical simulations by [20] demonstrated that networks with finite queue capacity cannot achieve queue stability using only MP signal control. This indicates that solely relying on MP signal control is inadequate for maximizing throughput in networks where queue capacity is limited. To address this, Gregoire et al. [40] improved MP control by integrating link queue capacity awareness that eliminates queue overflow while maintaining work conservation. Similarly, Mercader et al. [41] used travel time instead of queue lengths as the input of MP control to consider finite queue capacity. However, none of these studies have provided analytical proof of network stability under these modifications. As a result, the efficacy of these modified algorithms in real-world scenarios, particularly in today's frequently oversaturated and spillback-prone networks, remains uncertain. This highlights a significant research gap, as the assumption of infinite queue capacity is impractical for real-world applications.

Furthermore, current studies extending MP signal control have not integrated inflow regulation to ensure that demand does not exceed network capacity. According to the macroscopic fundamental diagram (MFD) theory, trip completion rates initially rise with demand until reaching a critical density point, beyond which they decline with further demand increase [42]. This theory suggests that in oversaturated networks (i.e., when cumulative flow surpasses the critical point), no signal control algorithm can effectively alleviate congestion or improve network throughput. Tsitsokas et al. [43] addressed this issue by integrating MP signal control and MFD-based perimeter control, adjusting inflows and outflows between regions to prevent regional oversaturation and enhance overall network performance. However, like many perimeter control studies, such as, [44], [45], and [46], they divided networks into fixed regions based on MFD characteristics, failing to dynamically address evolving congestion and local congestion issues. Li et al. [39] attempted to address these limitations by introducing location-varying cordons in perimeter control. However, this method still struggles with the fundamental limitations of MFD-based strategies, which belong to aggregate control and focus on the macroscopic flow–density relationship of urban networks. This aggregated nature makes it difficult to adapt to dynamic, localized traffic conditions and evolving congestion patterns. Moreover, MFD assumes homogeneous congestion distribution within each region, which is a challenging condition in practical scenarios.

Perimeter control primarily adjusts inter-regional flows rather than controlling entry flows to prevent overall network oversaturation. When the network is already oversaturated, the role of perimeter control, which regulates the inter-regional flow rate to improve network throughput, becomes limited. Therefore, controlling entry flows at network boundaries is crucial for efficient network performance under finite queue capacity with MP signal control. Su et al. [47] proposed a hierarchical control framework combining reinforcement learning-based perimeter control at the upper layer and MP signal control at the lower layer. While this hierarchical control framework does not rely on MFD, it still bases its upper-layer control on aggregated flow, accumulation, and speed of all links within protected regions, and lacks analytical proof of network throughput maximization. In the field of communications, studies like those by [48], [49], and [50] have explored combining admission control at entry nodes with MP control at internal nodes. However, their approaches require data packets to queue at nodes according to origin-destination (O-D) pairs or destinations and rely on precise queue length information at each node. Such queueing structures are infeasible in traffic networks, where vehicles cannot be organized or stored based on their individual destinations or O–D pairs.

From the literature review, several critical gaps in research related to MP control are apparent. Firstly, there is a notable lack of analytical evaluation of how queue length estimation errors and mean turn ratio estimation errors degrade the average delay and network throughput under MP signal control. Secondly, there is a shortfall in existing research regarding a micro-level, non-aggregated admission control algorithm to prevent network oversaturation and adaptively ensure that demand input rates do not exceed network capacity. Thirdly, the field lacks a comprehensive theory for evaluating the performance of networks with finite queue capacity in terms of average delay and network throughput.

In response to the identified research gaps, this study explores joint admission and signal control at the network level, retaining the benefits of MP control including distributed control, no need for prior knowledge of demand arrival rates and analytically provable network performance. This study makes the following contributions:

1) To avoid performance degradation caused by network oversaturation, this study develops a micro-level and distributed joint admission and signal control algorithm for partially connected networks having finite queue capacity to adaptively update signal phases at intersections and adjust demand input rates at entry nodes in real time;

Compared with previous studies [18], [19], [20], [51], the joint control algorithm no longer relies on precise queue length or turn ratio information. Unlike [43], which combines MP signal control with MFD-based perimeter control, the proposed admission control directly regulates inflows at all network entry nodes rather than inter-regional flow rates determined by MFD characteristics. This enables the algorithm to maintain feasible demand levels within the network and prevent

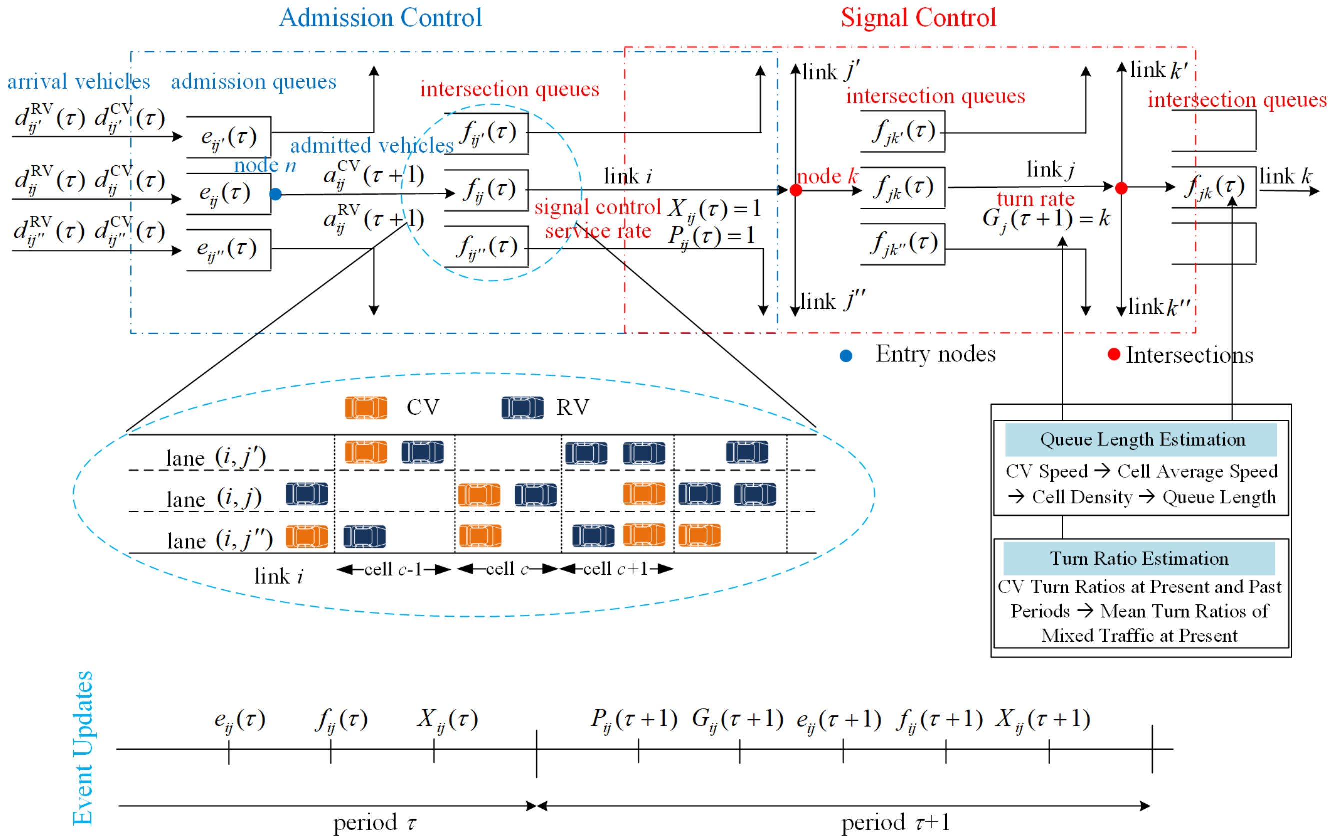

Fig. 1. A signalized network.

oversaturation, while capturing the microscopic queue dynamics instead of relying on aggregated macroscopic information.

2) This study develops a Lyapunov drift optimization algorithm to analytically prove a $[O(1/V), O(V)]$ tradeoff between throughput and delay for this joint control, and to analytically evaluate performance degradation bounds caused by estimation errors in queue lengths and mean turn ratios, where the parameter V is adjustable in accordance with finite queue capacity.

Compared with [39], this study analytically derives the performance degradation bounds of queue length estimation errors on network throughput and delay. In contrast to [40], [41], and [51], it further provides an analytical evaluation of how finite link capacity affects the throughput–delay relationship. Finally, unlike [48], [49], and [50] in the communication domain, where admission control and MP are jointly analyzed based on queues organized by O–D pairs or destinations, the Lyapunov drift optimization framework introduced in this study allows performance proof of the joint control algorithm without requiring such O–D or destination-based queuing structures.

The rest of this paper is organized as follows: Section II describes the research content. Section III outlines the models, including the network evolution, feasible phase, and throughput optimization models. Section IV presents the joint control algorithm and develops a Lyapunov drift optimization algorithm for performance proof. Section V presents numerical simulations to validate the effectiveness of joint control. Finally, Section VI concludes the study and suggests future research directions.

II. Problem Description

In signalized networks under mixed traffic conditions (see Fig. 1), this study focuses on the formulation of a stabilizing signal control strategy and the optimal allocation of demand input rates to ensure provable network performance. Input rates are regulated via distributed admission control at entry nodes, preventing network oversaturation while promoting equitable resource distribution. Admission control uses only the queue lengths at entry nodes and neighboring intersections, as depicted within the blue dotted outline. Simultaneously, distributed signal control at intersections contributes to network stability by maintaining queue lengths within prescribed queue capacity. The signal phases of each intersection are optimized by the MP-based signal control algorithm, which uses the queue lengths at connecting links, shown within the red dotted outline. The queue lengths and turn rates required for both strategies are estimated using feedback from CVs (see the flow charts within the black outline). This combined control strategy prevents network oversaturation, keeps real-time queue lengths within queue capacity, establishes a provable balance between average delay and network throughput, and ensures bounded network performance degradation caused by estimation errors. All network performance guarantees

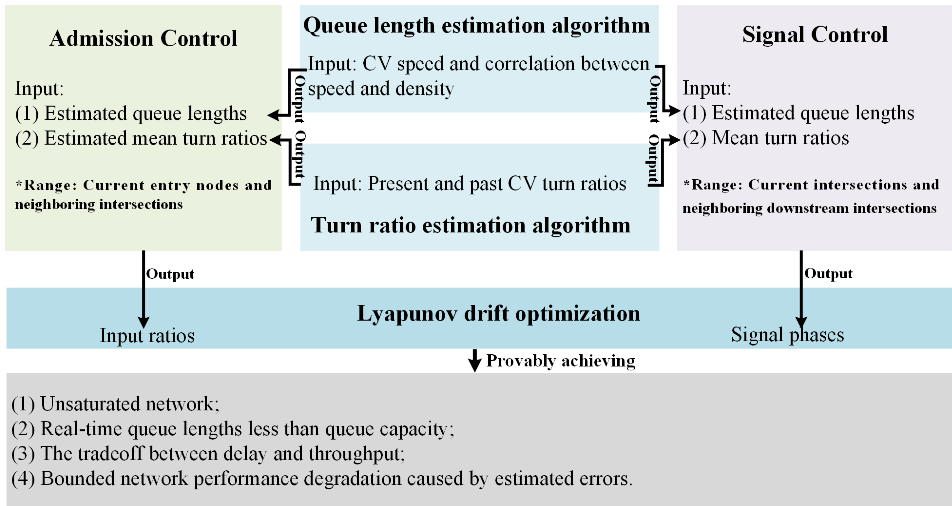

Fig. 2. Methodological framework.

are analytically proven using the developed Lyapunov drift optimization algorithm. The full methodological framework is shown in Fig. 2.

III. Model Construction

Section III-A models the evolution of the signalized network. Section III-B models the feasible signal phases and demand input rates. Finally, Section III-C develops a model to optimize network throughput subject to network stability.

A. Network Evolution

Following [20], the signalized network is represented using a store-and-forward queueing model, ignoring vehicle distribution along links. The network includes directed links $i \in \mathscr{I}_{all}$, entry nodes $n \in \mathbb{N}_{entry}$, and signalized intersections $n \in \mathbb{N}$. Vehicles, comprising CVs and RVs denoted as $m \in \mathscr{M} = \{\text{CV}, \text{RV}\}$, queue at entry nodes $n \in \mathbb{N}_{entry}$. Once admitted, they travel through entry, internal, and exit links ($i \in \mathscr{I}_{entry}$, $i \in \mathscr{I}$, and $i \in \mathscr{I}_{exit}$) before exiting the network. For clarity, $\mathscr{I}_{all} = \mathscr{I}_{entry} \cup \mathscr{I} \cup \mathscr{I}_{exit}$, representing all entry, internal, and exit links in the network. Time is divided into discrete periods $\tau = 1, 2, \ldots$, each with a fixed duration. The term $d_i^m(\tau)$ denotes the number of type m vehicles arriving at entry link $i \in \mathscr{I}_{entry}$ in period τ. Links departing from the terminal node of link i form the set $\mathscr{O}_i$, while those entering its starting node form the set $\mathscr{E}_i$. The non-negative iid (independent, identically distributed) variable $G_i(\tau)$ represents the turning ratio of the vehicles entering the link i at period τ. Its values correspond to downstream links $j \in \mathscr{O}_i$. At the start of period τ, $G_i(\tau)$ is updated and equals $j \in \mathscr{O}_i$, with an average given by the fixed but unknown mean turn ratios g_{ij}. If $G_i(\tau)$ equals j, then $G_{ij}(\tau)$ is set to 1; otherwise, it defaults to 0. These updates are illustrated at the bottom of Fig. 1. The update for the admission queue length $e_{ij}(\tau)$ is defined as follows:

$$e_{ij}(\tau+1) = e_{ij}(\tau) + \sum_{m \in \mathscr{M}} d_i^m(\tau+1) G_{ij}(\tau+1) - \sum_{m \in \mathscr{M}} a_{ij}^m(\tau+1), \forall i \in \mathscr{I}_{entry}, j \in \mathscr{O}_i \quad (1)$$

where $a_{ij}^m(\tau+1)$ denotes the number of type m vehicles admitted into the network through admission control at admission queue $e_{ij}(\tau)$ in period $(\tau+1)$. The details of $a_{ij}^m(\tau+1)$ are provided in the admission control algorithm design in Section IV-B. In period $(\tau+1)$, admission queue $e_{ij}(\tau)$ decreases by $\sum_{m \in \mathscr{M}} a_{ij}^m(\tau+1)$ as these vehicles enter the network and increases by $\sum_{m \in \mathscr{M}} d_i^m(\tau+1) G_{ij}(\tau+1)$ due to incoming vehicles.

After vehicles are admitted from the admission queues, their dynamics are governed by the entry-link queues. We now define how queues $f_{ij}(\tau)$ on entry links $i \in \mathscr{I}_{entry}$ evolve. The iid random variable $P_{ij}(\tau+1)$ denotes the realized flow rate in period $(\tau+1)$ and averages to the known saturation flow rate p_{ij} for turn (i, j) with $j \in \mathscr{O}_i$. As depicted at the bottom of Fig. 1, $P_{ij}(\tau+1)$ is updated at the start of period $(\tau+1)$. If the signal control variable $X_{ij}(\tau)$ equals 1 at the end of τ, its corresponding turn from link i to j is actuated in period $(\tau+1)$. Consequently, up to $P_{ij}(\tau+1)$ vehicles from queue $f_{ij}(\tau)$ are processed during period $(\tau+1)$. The formula for updating the queue lengths on entry links $i \in \mathscr{I}_{entry}$ is defined as follows:

$$f_{ij}(\tau+1) = f_{ij}(\tau) - \left[P_{ij}(\tau+1) X_{ij}(\tau) \wedge f_{ij}(\tau)\right] + \sum_{m \in \mathscr{M}} a_{ij}^m(\tau+1), \forall i \in \mathscr{I}_{entry}, j \in \mathscr{O}_i \quad (2)$$

where $z \wedge y$ is a function representing the minimum of z and y (i.e., $\min[z, y]$). The second term shows that the queue $f_{ij}(\tau)$ decreases by $\min[P_{ij}(\tau+1), f_{ij}(\tau)]$ during period $(\tau+1)$ if the turn (i, j) is active. This means that when $X_{ij}(\tau)$ equals 1, up to $\min[P_{ij}(\tau+1), f_{ij}(\tau)]$ vehicles leave the queue $f_{ij}(\tau)$ during period $(\tau+1)$; otherwise, no vehicles leave. The final term $\sum_{m \in \mathscr{M}} a_{ij}^m(\tau+1)$ represents the vehicles admitted from admission queues to the queue $f_{ij}(\tau)$ during period $(\tau+1)$.

Unlike entry links, where queues are formed by input vehicles, queues on internal links $i \in \mathscr{I}$ are fed by upstream intersections. When $G_i(\tau+1)$ equals j (or equivalently $G_{ij}(\tau+1)$ equals 1), vehicles leave the queue $f_{ki}(\tau)$ from upstream link $k \in \mathscr{E}_i$ and join queue $f_{ij}(\tau)$. The update equation for queues

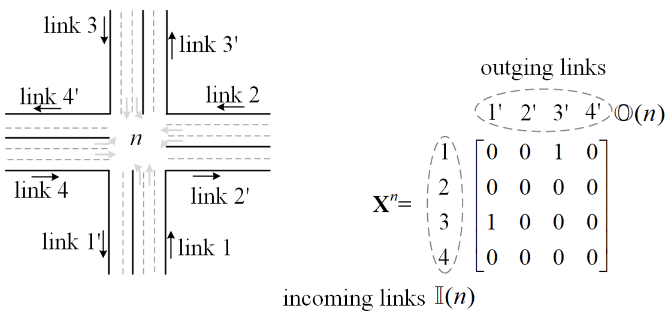

Fig. 3. Intersection n and control matrix $\mathbf{X}^n$ for the phase formed by turns $(3, 1')$ and $(1, 3')$.

on internal links $i \in \mathscr{I}$ is defined as follows:

$$f_{ij}(\tau+1) = f_{ij}(\tau) - \left[P_{ij}(\tau+1)X_{ij}(\tau) \wedge f_{ij}(\tau)\right] + \sum_{k \in \mathscr{E}_i} \left[P_{ki}(\tau+1)X_{ki}(\tau) \wedge f_{ki}(\tau)\right] G_{ij}(\tau+1) \quad \forall i \in \mathscr{I}, j \in \mathscr{O}_i \tag{3}$$

where the second term echoes that of Eq. (2), indicating a reduction in $f_{ij}(\tau)$ by $\min[P_{ij}(\tau+1), f_{ij}(\tau)]$ during period $(\tau+1)$ when turn (i, j) is active (i.e., $X_{ij}(\tau) = 1$). The third term details the vehicles joining queue $f_{ij}(\tau)$ from upstream intersections during period $(\tau+1)$.

B. Modeling Feasible Signal Phases and Demand

We identify the allowable concurrent turns at intersections and their corresponding saturation flow rates. The sets of outgoing and incoming links at an intersection $n \in \mathbb{N}$ are denoted as $\mathbb{O}(n)$ and $\mathbb{I}(n)$, respectively. Intersection $n \in \mathbb{N}$ accommodates the set of turning pairs $\{(i, j) \in \mathbb{I}(n) \times \mathbb{O}(n)\}$. Selected subsets of these turns can be activated simultaneously, forming a phase represented by the matrix $\mathbf{X}^n = \{X^n_{ij}, i \in \mathbb{I}(n), j \in \mathbb{O}(n)\}$. The element $X^n_{ij}(\tau)$ is set to 1 if turn (i, j) is active during τ, and 0 otherwise. All such matrices $\mathbf{X}^n$ at intersection $n \in \mathbb{N}$ form the set $\mathbb{X}^n$. Fig. 3 illustrates an isolated intersection where turns $(3, 1')$ and $(1, 3')$ can be activated simultaneously, forming a phase on the right.

All individual intersection matrices $\mathbf{X}^n$ can be merged to form the network control matrix $\mathbf{X} = \{X_{ij}, i \in \mathscr{I}_{entry} \cup \mathscr{I}, j \in \mathscr{I} \cup \mathscr{I}_{exit}\}$, representing the activation status of turns across the entire network. In line with [20], $\mathbf{X}$ is arranged in a block-diagonal manner, with the matrices $\mathbf{X}^n$ along the diagonal and zeroes elsewhere. Each element X_{ij} in $\mathbf{X}$ corresponds to the activation status of turn (i, j) at its associated intersection, such that $X_{ij}(\tau) = 1$ if $X^n_{ij}(\tau) = 1$, and $X_{ij} = 0$ otherwise. All such matrices $\mathbf{X}$ form the set $\mathbb{X}$. To determine the saturation flow rate of each turn, the convex hull $co(\mathbb{X}) = \left\{\sum_{\mathbf{X}\in\mathbb{X}} \lambda_{\mathbf{X}}\mathbf{X} \middle| \lambda_{\mathbf{X}} \geq 0, \sum_{\mathbf{X}\in\mathbb{X}} \lambda_{\mathbf{X}} = 1\right\}$ of set $\mathbb{X}$ is defined, where $\lambda_{\mathbf{X}}$ represents the weight coefficient of matrix $\mathbf{X}$. Since $\mathbb{X}$ is finite, $co(\mathbb{X})$ forms a bounded, closed polytope. We can deduce the below proposition:

Proposition 1: If it is possible to find a control sequence $\{\mathbf{X}(1), \ldots, \mathbf{X}(\tau), \ldots\}$ such that the equation $\lim_{T\to\infty} \frac{1}{T}\sum_{\tau=0}^{T-1} X_{ij}(\tau) = \Upsilon_{ij}$ holds for all turns (i, j) with $i \in \mathscr{I}_{entry} \cup \mathscr{I}$ and $j \in \mathscr{I} \cup \mathscr{I}_{exit}$, the matrix $\boldsymbol{\Upsilon} = \{\Upsilon_{ij}, i \in \mathscr{I}_{entry} \cup \mathscr{I}, j \in \mathscr{I} \cup \mathscr{I}_{exit}\}$ is contained within convex hull $co(\mathbb{X})$, expressed as $\boldsymbol{\Upsilon} \in co(\mathbb{X})$.

If a matrix $\mathbf{X}'$ is derived by turning certain elements of a matrix $\mathbf{X} \in \mathbb{X}$ to zero, then $\mathbf{X}'$ remains within $\mathbb{X}$. In simple terms, it is permissible when no turn is actuated. Consequently, a matrix $\boldsymbol{\Upsilon}' = \{\Upsilon'_{ij}, i \in \mathscr{I}_{entry} \cup \mathscr{I}, j \in \mathscr{I} \cup \mathscr{I}_{exit}\}$ derived from such a permissible sequence $\{\mathbf{X}'(1), \ldots, \mathbf{X}'(\tau), \ldots\}$, which averages over time to Υ'_{ij} (i.e., $\lim_{T\to\infty} \frac{1}{T}\sum_{\tau=0}^{T-1} X'_{ij}(\tau) = \Upsilon'_{ij}$), satisfies $0 \leq \boldsymbol{\Upsilon}' \leq \boldsymbol{\Upsilon}$. If $\boldsymbol{\Upsilon}$ belongs to the convex hull $co(\mathbb{X})$, $\boldsymbol{\Upsilon}'$ also belongs to it (i.e., $\boldsymbol{\Upsilon}' \in co(\mathbb{X})$). The element Υ_{ij} in matrix $\boldsymbol{\Upsilon}$, as defined in Proposition 1, represents the average actuation rate of each turn during one period under control sequence $\{\mathbf{X}(1), \ldots, \mathbf{X}(\tau), \ldots\}$. Therefore, the saturated service flow rate of each turn in one period is $\Upsilon_{ij} p_{ij}$ with $i \in \mathscr{I}_{entry} \cup \mathscr{I}$ and $j \in \mathscr{I} \cup \mathscr{I}_{exit}$. According to Proposition 1, feasible demand must ensure that the flow rate at each turn does not exceed its saturated service flow rate.

Before defining feasible demand, we first define network stability. Vehicles in admission queues are outside the network and do not affect its stability or throughput. Network stability focuses only on the queues at signalized intersections and does not include vehicles waiting at entry nodes. Following [49], network stability is defined as follows:

Definition 1 (Network Stability): The queuing network, symbolized by $\mathbf{F}(\tau) = \{f_{ij}(\tau), i \in \mathscr{I}_{entry} \cup \mathscr{I}, j \in \mathscr{O}_i\}$, is considered strongly stable in the mean if the time-averaged expected lengths of all queues at intersections remain bounded, i.e., $\lim_{T\to\infty} \frac{1}{T}\sum_{\tau=0}^{T-1} \sum_{i\in\mathscr{I}_{entry}\cup\mathscr{I}} \sum_{j\in\mathscr{O}_i} E\left\{f_{ij}(\tau)\right\} < \infty$, where $E\{\cdot\}$ denotes the expectation function.

Based on Definition 1, whether signal control can stabilize intersection queues depends only on the input rate vector $\vec{\mathscr{A}}^m = \{\bar{a}^m_1, \ldots, \bar{a}^m_i, \ldots, \bar{a}^m_J\}$ and not the arrival rate vector $\vec{\mathscr{D}}^m = \{\bar{d}^m_1, \ldots, \bar{d}^m_i, \ldots, \bar{d}^m_J\}$ for each vehicle type $m \in \mathscr{M}$. Here, $a^m_i(\tau)$ and $d^m_i(\tau)$ denote, respectively, the number of type-m vehicles admitted into and arriving at entry link $i \in \mathscr{I}_{entry}$ during period τ. The time-averaged expected input rate $\bar{a}^m_i$ is then defined as $\lim_{T\to\infty} \frac{1}{T}\sum_{\tau=0}^{T-1} E\{a^m_i(\tau)\}$, and the expected arrival rate $\bar{d}^m_i$ is defined as $E\{d^m_i(\tau)\}$. J indicates the total number of entry links. Since input vehicles come solely from arrivals, $\vec{\mathscr{A}}^m$ cannot exceed $\vec{\mathscr{D}}^m$. Given the fixed average turn ratios (i.e., the predefined mean routing proportion matrix $\mathbf{G} = \{g_{ij}, i \in \mathscr{I}_{entry} \cup \mathscr{I}, j \in \mathscr{I} \cup \mathscr{I}_{exit}\}$), we can define a matrix $\mathbf{H}$ based on $\mathbf{G}$ to establish a correspondence between the input rate vector $\vec{\mathscr{A}}^m = \left\{\bar{a}^m_i, i \in \mathscr{I}_{entry}\right\}$ and the flow rate vector on all links $\vec{\mathscr{H}}^m = \left\{\bar{h}^m_i, i \in \mathscr{I}_{all}\right\}$. This relationship is presented in the following proposition:

Proposition 2: For any vehicle type $m \in \mathscr{M}$, an input rate vector $\vec{\mathscr{A}}^m = \left\{\bar{a}^m_i, i \in \mathscr{I}_{entry}\right\}$ corresponds to a specific flow rate vector $\vec{\mathscr{H}}^m = \left\{\bar{h}^m_i, i \in \mathscr{I}_{all}\right\}$. The relationship between $\bar{a}^m_i$

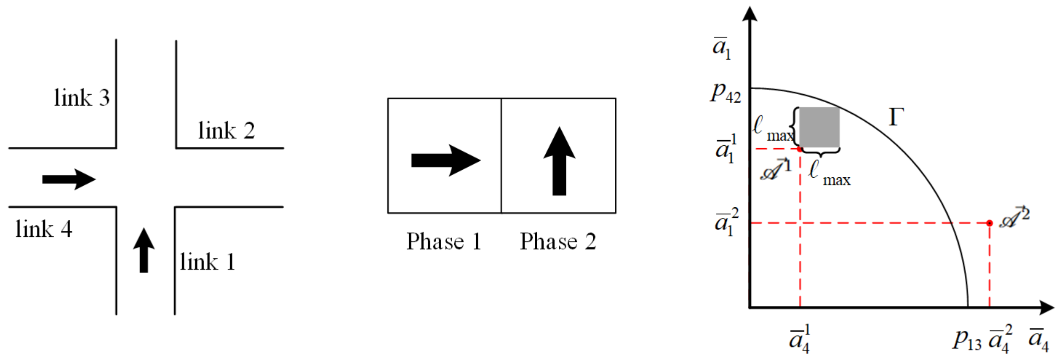

Fig. 4. Isolated intersection: Layout (left), phases (middle), and capacity region (right).

and $\bar{h}_i^m$ is established through the matrix $\mathbf{H}$ (i.e., $\vec{\mathscr{H}}^m = \vec{\mathscr{A}}^m\mathbf{H}$), which is derived from the predefined mean routing proportion matrix $\mathbf{G}$. Specifically, for $i \in \mathscr{I}_{entry}$, $\bar{h}_i^m$ equals $\bar{a}_i^m$, while for $i \in \mathscr{I} \cup \mathscr{I}_{exit}$, $\bar{h}_i^m$ equals $\sum_{k\in\mathscr{E}_i} \bar{h}_k^m g_{ki}$.

Building on Proposition 2, we introduce the following propositions to define the feasible demand input rates:

Proposition 3: Let Γ be the set of feasible demand input rates $\vec{\mathscr{A}} = \{\bar{a}_i, i \in \mathscr{I}_{entry}\}$, consisting of input rate vectors for all vehicle types (i.e., $\vec{\mathscr{A}} = \sum_{m\in\mathscr{M}} \vec{\mathscr{A}}^m$ and $\bar{a}_i = \sum_{m\in\mathscr{M}} \bar{a}_i^m$ with $i \in \mathscr{I}_{entry}$), also referred to as the capacity region. For $\vec{\mathscr{H}}^m = \vec{\mathscr{A}}^m\mathbf{H}$ with $m \in \mathscr{M}$, there exists a constant ℓ within the range 0 to $\ell_{\max}$ and a matrix $\mathbf{\Upsilon} = \{\Upsilon_{ij}\} \in co(\mathbb{X})$ such that the inequality $\sum_{m\in\mathscr{M}} \bar{h}_i^m g_{ij} + \ell \le p_{ij}\Upsilon_{ij}$ holds for all $i \in \mathscr{I}_{entry} \cup \mathscr{I}$ and $j \in \mathscr{I} \cup \mathscr{I}_{exit}$. $\ell_{\max}$ denotes the maximum potential buffer, which diminishes as the vector $\vec{\mathscr{A}}$ gets closer to the boundary of Γ.

Proposition 4: If a non-negative vector $\vec{\mathscr{A}}'$ does not exceed a feasible input rate $\vec{\mathscr{A}}$ (i.e., $\vec{\mathscr{A}} \in \Gamma$), then $\vec{\mathscr{A}}'$ also falls within the capacity region Γ.

The concept of Γ is illustrated further in Fig. 4, which depicts an intersection with four unidirectional links, two signal phases, and two turning movements (from link 4 to link 2 and from link 1 to link 3). The input rate $\vec{\mathscr{A}}^1 = \{\bar{a}_1^1, \bar{a}_4^1\}$ lies within the feasible region Γ, where $\bar{a}_1^1$ and $\bar{a}_4^1$ denote the time-averaged expected input rates of links 1 and 4, respectively. According to Proposition 3, there exists a bounded positive constant ℓ (i.e., $0 < \ell < \ell_{\max}$) such that the inequalities $\sum_{m\in\mathscr{M}} \bar{h}_1^m g_{13} + \ell \le p_{13}\Upsilon_{13}$ and $\sum_{m\in\mathscr{M}} \bar{h}_4^m g_{42} + \ell \le p_{42}\Upsilon_{42}$ hold. Here, the link flow rates $\sum_{m\in\mathscr{M}} \bar{h}_1^m$ and $\sum_{m\in\mathscr{M}} \bar{h}_4^m$ correspond to the input rates $\bar{a}_1^1$ and $\bar{a}_4^1$, respectively, and both turning ratios g_{13} and g_{42} are equal to 1. Hence, ℓ represents the available network reserve capacity. Conversely, the input rate $\vec{\mathscr{A}}^2 = \{\bar{a}_1^2, \bar{a}_4^2\}$ lies outside the feasible region Γ. In this case, $\bar{a}_1^2$ and $\bar{a}_4^2$ represent higher time-averaged expected input rates of links 1 and 4 that violate the above inequalities, indicating that the corresponding demand levels exceed intersection capacity and thus cannot be stabilized.

C. Optimization Model Construction

In accordance with the problem description, the optimization model for maximizing network throughput uses the input rate vector $\vec{\mathscr{A}}^m = \{\bar{a}_1^m, \ldots, \bar{a}_i^m, \ldots, \bar{a}_J^m\}$ for each vehicle type $m \in \mathscr{M}$. The time-averaged expected input rate for a vehicle type $m \in \mathscr{M}$ entering queue $f_{ij}(\tau)$ on entry link $i \in \mathscr{I}_{entry}$ is defined as $\bar{a}_{ij}^m = \lim_{T\to\infty} \frac{1}{T}\sum_{\tau=0}^{T-1} E\{a_{ij}^m(\tau)\}$. Using the mean routing proportion matrix $\mathbf{G}$ from Proposition 2, this rate can be expressed as $\bar{a}_{ij}^m = \bar{a}_i^m g_{ij}$. The term $\hbar_{ij}$ serves as the weighting factor for the total input rate $\sum_{m\in\mathscr{M}} \bar{a}_{ij}^m$. The optimization model to maximize the weighted network throughput subject to network stability is constructed as follows:

$$\max \sum_{i\in\mathscr{I}_{entry}} \sum_{j\in\mathscr{O}_i} \sum_{m\in\mathscr{M}} \hbar_{ij}\bar{a}_{ij}^m \tag{4}$$

$$\textbf{s.t.} \lim_{T\to\infty} \frac{1}{T}\sum_{\tau=0}^{T-1} \sum_{i\in\mathscr{I}_{entry}\cup\mathscr{I}} \sum_{j\in\mathscr{O}_i} E\left\{f_{ij}(\tau)\right\} < \infty \tag{5}$$

$$\sum_{m\in\mathscr{M}} \vec{\mathscr{A}}^m \in \Gamma \tag{6}$$

As stated in Eq. (4), the model aims to maximize the weighted throughput. Eq. (5) ensures network strong stability as defined in Definition 1. Additionally, Eq. (6) ensures that the input rate remains feasible.

Although the above optimization model can theoretically be solved using the known arrival rate $\vec{\mathscr{D}}^m = \{\bar{d}_1^m, \ldots, \bar{d}_i^m, \ldots, \bar{d}_J^m\}$ for each vehicle type $m \in \mathscr{M}$ and capacity region Γ, accurately determining these parameters in advance is challenging for large-scale networks. Even without admission control, solving for the variables $X_{ij}(\tau)$ with $i \in \mathscr{I}_{entry} \cup \mathscr{I}$ and $j \in \mathscr{O}_i$ in each period τ is complex due to their interactions. To overcome these challenges, the next section introduces an implementable algorithm based on MP control to achieve near-maximum throughput while keeping average delay within acceptable limits.

IV. Joint Control Algorithm Design and Performance Analysis

Section IV-A introduces the algorithms for real-time estimations of queue lengths and mean turn ratios. Subsequently, Section IV-B presents an implementable joint admission and signal control (JASC) algorithm. Section IV-C then evaluates the effectiveness of the JASC algorithm.

A. Estimating of Queue Lengths and Mean Turn Ratios

Based on the issues identified in Section II, the MP-based signal control and admission control discussed in this study rely on queue length data, representing the number of vehicles on specific lanes. However, due to limited connectivity in the short term, accurately monitoring vehicle counts on each lane at every moment is difficult. To address this, we apply the traffic state reconstruction method proposed by [52], which uses interpolation technology for real-time queue length estimation. The core idea is to calculate the speed at various locations by combing both current and historical speed data, weighted by their collection points and timestamps. Speed data from CVs at selected cells along a lane (see Fig. 1) are used to approximate average speed at other cells. Using the known relationship between traffic density and speed, these speed estimates are converted to traffic density, enabling the estimation of total vehicle counts, including both CVs and RVs. *It is important to note that any real-time queue length estimation algorithm can be used. Many real-time queue length estimation methods have been developed, including those based on connected vehicle data, video detection, and model- or interpolation-based estimation [53], [54]. Readers may refer to recent reviews and implementations for detailed methodologies and comparative performance analyses [55], [56]. Since this study focuses on analyzing the impact of queue length estimation errors on network performance degradation under MP-based control, a simple interpolation-based method is adopted.*

In accordance with Fig. 1, the lane (i, j) with $i \in \mathscr{I}_{entry} \cup \mathscr{I}$ and $j \in \mathscr{O}_i$ is divided into discrete cells indexed by c. Let $\wp_{ij}$ be the set of all cells c on lane (i, j). The distance from the center position of cell $c \in \wp_{ij}$ to the upstream end of the lane (i, j) is denoted as x_{ij}^c. Let τ_c be the period when the CV in cell c transmits the latest speed data. For simplicity, τ_c also refers to the period when the average velocity of mixed traffic in cell c is estimated. To calculate the average speed at a specific location and time within the cell, denoted by the cell-time pair (x_{ij}^c, τ_c), we assign a weight to the speed data $v_{ij}^k\left(x_{ij}^k, \tau_k\right)$ from another cell-time pair (x_{ij}^k, τ_k) as follows:

$$\varphi_{ij}^k(x_{ij}^c, \tau_c) = \frac{\nu\left(x_{ij}^k - x_{ij}^c, \tau_k - \tau_c\right)}{\sum_{l \in \wp_{ij}} \nu\left(x_{ij}^l - x_{ij}^c, \tau_l - \tau_c\right)}$$
$$\forall i \in \mathscr{I}_{entry} \cup \mathscr{I}, j \in \mathscr{O}_i, k \in \wp_{ij} \tag{7}$$

where the kernel function $\nu\left(x_{ij}^k - x_{ij}^c, \tau_k - \tau_c\right)$ is defined as $\exp\left\{-\frac{\left|x_{ij}^k - x_{ij}^c\right|}{\psi} - \frac{\tau_k - \tau_c}{\iota}\right\}$ based on [39]. $\psi > 0$ and $\iota > 0$ are smoothing parameters representing the spatial and temporal decay scales, respectively. A smaller ψ gives higher sensitivity to spatial differences, while a smaller ι assigns more weight to recent observations.

Based the interpolation technology proposed by [52], the average speed at the cell-time pair $\left(x_{ij}^c, \tau_c\right)$ is estimated as:

$$v_{ij}^c\left(x_{ij}^c, \tau_c\right) = \sum_{l \in \wp_{ij}} \varphi_{ij}^l(x_{ij}^c, \tau_c) v_{ij}^l\left(x_{ij}^l, \tau_l\right)$$
$$\forall i \in \mathscr{I}_{entry} \cup \mathscr{I}, j \in \mathscr{O}_i, c \in \wp_{ij} \tag{8}$$

According to the Newell-Franklin speed-density relation in [39], the density at the cell-time pair $\left(x_{ij}^c, \tau_c\right)$ is given by:

$$\rho_{ij}^c\left(x_{ij}^c, \tau_c\right) = \frac{\rho_{ij}^{jam}}{1 - \frac{v_{ij}^{free}}{\upsilon_{ij}} \ln\left(1 - \frac{v_{ij}^c\left(x_{ij}^c, \tau_c\right)}{v_{ij}^{free}}\right)}$$
$$\forall i \in \mathscr{I}_{entry} \cup \mathscr{I}, j \in \mathscr{O}_i, c \in \wp_{ij} \tag{9}$$

where υ_{ij} represents the shockwave speed, ρ_{ij}^{jam} denotes the congestion density, and v_{ij}^{free} denotes the free flow speed.

The real-time estimate $\hat{f}_{ij}(\tau)$ of the queue length $f_{ij}(\tau)$ is given as follows:

$$\hat{f}_{ij}(\tau) = \sum_{c \in \wp_{ij}} \rho_{ij}^c\left(x_{ij}^c, \tau_c\right) D_{ij}^c, \forall i \in \mathscr{I}_{entry} \cup \mathscr{I}, j \in \mathscr{O}_i \tag{10}$$

where D_{ij}^c is the length of cell c on lane (i, j). Here, we assume uniform density at every point within a given cell.

The study by [39] suggests using the intersection service rate $P_{ij}(\tau)$ to fine-tune the queue length estimations $\hat{f}_{ij}(\tau)$ for improved accuracy. However, since the service rate remains relatively stable except during disruptions, we ignore this adjustment. This means that the adjusted queue length $\tilde{f}_{ij}(\tau)$ is set equal to the real-time estimation, i.e., $\tilde{f}_{ij}(\tau) = \hat{f}_{ij}(\tau)$. To examine the effects of queue length estimation errors on average delay and network throughput, we define the relationship between the adjusted queue length $\tilde{f}_{ij}(\tau)$ and the actual queue length $f_{ij}(\tau)$ (measured in a fully connected environment) as follows:

$$\omega_{ij}(\tau) = \tilde{f}_{ij}(\tau) - f_{ij}(\tau), \forall i \in \mathscr{I}_{entry} \cup \mathscr{I}, j \in \mathscr{O}_i \tag{11}$$

where $\omega_{ij}(\tau)$ is the estimation error at period τ. We define matrices $\widehat{\boldsymbol{F}}(\tau) = \left\{\hat{f}_{ij}(\tau), i \in \mathscr{I}_{entry} \cup \mathscr{I}, j \in \mathscr{O}_i\right\}$, $\boldsymbol{\Omega}(\tau) = \left\{\omega_{ij}(\tau), i \in \mathscr{I}_{entry} \cup \mathscr{I}, j \in \mathscr{O}_i\right\}$, and $\widetilde{\boldsymbol{F}}(\tau) = \left\{\tilde{f}_{ij}(\tau), i \in \mathscr{I}_{entry} \cup \mathscr{I}, j \in \mathscr{O}_i\right\}$ to simplify the proof below.

Next, we design the turn rate estimation algorithm. Let $\widehat{G}_{ij}(\tau)$ represent the turn rate reported by CVs from link i to link j during period τ. We assume that the mean turn ratios of CVs and RVs are identical and constant, allowing us to simplify by assuming that the turn ratio from CVs matches the mixed turn ratio $G_{ij}(\tau)$ for both RVs and CVs. The fixed but unknown mean turn ratio g_{ij} represents the expected value of $\widehat{G}_{ij}(\tau)$ when queue evolution is in a stationary state. Let $\widetilde{G}_{ij}(\tau)$ be the estimated value of g_{ij} at the start of period τ. When queues are positive recurrent, reliable estimators $\widetilde{G}_{ij}(\tau)$ can be maintained through simple averaging and remain close to g_{ij} [34]. Following [34], we use exponential averaging to update $\widetilde{G}_{ij}(\tau)$ as follows:

$$\widetilde{G}_{ij}(\tau) = (1 - \lambda)\widetilde{G}_{ij}(\tau - 1) + \lambda\widehat{G}_{ij}(\tau) \tag{12}$$

where λ is a smoothing factor. For clarity in subsequent theoretical proofs, we define the matrices $\widetilde{\mathbf{G}}(\tau) = \left\{\widetilde{G}_{ij}(\tau), i \in \mathscr{I}_{entry} \cup \mathscr{I}, j \in \mathscr{I} \cup \mathscr{I}_{exit}\right\}$ and $\widehat{\mathbf{G}}(\tau) = \left\{\widehat{G}_{ij}(\tau), i \in \mathscr{I}_{entry} \cup \mathscr{I}, j \in \mathscr{I} \cup \mathscr{I}_{exit}\right\}$.

B. JASC Algorithm Design

The independent admission control and signal control in the JASC algorithm are introduced as follows:

1) Admission Control: If the modified queue length $\tilde{f}_{ij}(\tau)$ on entry link $i \in \mathscr{I}_{entry}$ does not exceed $\frac{V\hbar_{ij}-2\hat{\omega}}{2}$ by the end of period τ, then $[a_{ij}^M \wedge e_{ij}(\tau)]$ vehicles from the admission queue $e_{ij}(\tau)$ are allowed to merge into queue $f_{ij}(\tau)$ in period $(\tau+1)$. Conversely, if $\tilde{f}_{ij}(\tau)$ exceeds this threshold, no vehicles are allowed to enter in period $(\tau+1)$. Therefore, the total number $\sum_{m\in\mathscr{M}} a_{ij}^m(\tau+1)$ of vehicles permitted to enter the network in the next period $(\tau+1)$ is determined as follows:

$$\sum_{m\in\mathscr{M}} a_{ij}^m(\tau+1) = \begin{cases} a_{ij}^M \wedge e_{ij}(\tau), & \text{if } \tilde{f}_{ij}(\tau) \le \frac{V\hbar_{ij}-2\hat{\omega}}{2} \\ 0, & \text{otherwise} \end{cases} \tag{13}$$

The threshold $\frac{V\hbar_{ij}-2\hat{\omega}}{2}$ is explained in the design principles of JASC algorithm in Section IV-C. V is a positive parameter chosen to prevent queue overflow based on queue capacity, with its selection detailed in Theorem 2. The parameter $\hat{\omega}$ represents the maximum queue length estimation error of $\omega_{ij}(\tau)$ across all periods and links, defined as $\hat{\omega} = \max_{i\in\mathscr{I}_{entry}\cup\mathscr{I}, j\in\mathscr{O}_i, \tau} \omega_{ij}(\tau)$. The saturation input rate a_{ij}^M is predetermined based on the entry structure.

2) Signal Control: The network signal control matrix $\mathbf{X}(\tau) = \{X_{ij}(\tau)\}$ is solved by the end of period τ through the following optimization problem:

$$\max \sum_{i\in\mathscr{I}_{entry}\cup\mathscr{I}} \sum_{j\in\mathscr{O}_i} p_{ij} w_{ij}\left(\widetilde{\mathbf{F}}(\tau)\right) X_{ij}(\tau) \tag{14}$$

$$\textbf{s.t.} \quad \mathbf{X}(\tau) = \{X_{ij}(\tau)\} \in \mathbb{X} \tag{15}$$

where the weight $w_{ij}\left(\widetilde{\mathbf{F}}(\tau)\right)$ of turn (i, j) is defined as $\tilde{f}_{ij}(\tau) - \sum_{k\in\mathscr{O}_j} \widetilde{G}_{jk}(\tau+1)\tilde{f}_{jk}(\tau)$.

In the aforementioned optimization model, the signal control decisions at each intersection are independent, allowing the control matrix $\mathbf{X}^n(\tau) = \{X_{ij}^n(\tau)\}$ for each intersection $n \in \mathbb{N}$ to be solved separately as follows:

$$\max \sum_{i\in\mathbb{I}(n)} \sum_{j\in\mathbb{O}(n)} p_{ij} w_{ij}\left(\widetilde{\mathbf{F}}(\tau)\right) X_{ij}^n(\tau) \tag{16}$$

$$\textbf{s.t.} \quad \mathbf{X}^n(\tau) = \{X_{ij}^n(\tau)\} \in \mathbb{X}^n \tag{17}$$

Solving the optimization problem is straightforward since $w_{ij}\left(\widetilde{\mathbf{F}}(\tau)\right)$ and p_{ij} are predetermined. Given the finite set $\mathbb{X}^n$, the optimal solution can be found by examining each matrix in the set. Moreover, the signal control algorithm avoids cross-interference among decisions in each period, ensuring that decisions remain independent.

Remark 1: Varaiya [20] initially introduced an MP signal control algorithm that uses the optimization models in Eqs. (14) and (15) for real-time signal phase updates. In these models, the weight $w_{ij}(\tau)$ (i.e., $w_{ij}(\tau) = f_{ij}(\tau) - \sum_{k\in\mathscr{O}_j} g_{ij} f_{ij}(\tau)$) for each turn depends heavily on the exact queue length $\mathbf{F}(\tau)$ and the average turn ratio $\mathbf{G}$, which are difficult to measure without fully connectivity. Such widespread connectivity is unlikely in the near future. The models in this paper use estimated turn ratios $\widetilde{\mathbf{G}}(\tau)$ and queue lengths $\widetilde{\mathbf{F}}(\tau)$ to reduce the dependence on a fully connected environment.

Section IV-C provides a detail discussion of the design principles behind JASC. Here, we focus on presenting its performance:

Theorem 2: The JASC algorithm yields the following outcomes for any demand arrival rate $\vec{\mathscr{D}}^m$ with $m \in \mathscr{M}$:

1) Network throughput meets the following lower bound:

$$\sum_{i\in\mathscr{I}_{entry}} \sum_{j\in\mathscr{O}_i} \sum_{m\in\mathscr{M}} \hbar_{ij}\bar{a}_{ij}^m \ge -\frac{3MK^2 + 4\varkappa + 4\kappa}{V} + \sum_{i\in\mathscr{I}_{entry}} \sum_{j\in\mathscr{O}_i} \sum_{m\in\mathscr{M}} \hbar_{ij}\bar{a}_i^{m*} g_{ij} \tag{18}$$

where M denotes the number of intersection queues. K represents the maximum of P_{ij}^M and a_{ij}^M across all entry and internal link pairs, defined as $K = \max_{i\in\mathscr{I}_{entry}\cup\mathscr{I}, j\in\mathscr{O}_i} \left[\sum_i P_{ij}^M, a_{ij}^M\right]$, where P_{ij}^M is the maximum value of $P_{ij}(\tau)$ over all periods and a_{ij}^M is defined in Eq. (13). The term $\varkappa$ is defined as $\sum_{i\in\mathscr{I}_{entry}\cup\mathscr{I}} \sum_{j\in\mathscr{O}_i} p_{ij}\left(\hat{\omega} + \sum_{k\in\mathscr{O}_j} \hat{\omega} g_{jk}\right)$, and κ is defined as $\hat{\omega} \sum_{i\in\mathscr{I}_{entry}} \sum_{j\in\mathscr{O}_i} \sum_{m\in\mathscr{M}} \bar{a}_i^{m*} g_{ij}$. These terms measure the impact of queue length estimate errors on network throughput caused by signal control and admission control, respectively. The optimal input rate $\bar{a}_i^{m*}$ of vehicle type $m \in \mathscr{M}$ at entry link $i \in \mathscr{I}_{entry}$ assists in the comparative analysis of throughput achieved by the JASC algorithm against the theoretical optimum. The corresponding optimal input rate $\bar{a}_{ij}^{m*}$ equals $\bar{a}_i^{m*} g_{ij}$ and can theoretically be solved by the optimization models in Eqs. (4)–(6). However, this optimal rate is used for comparison purposes and is not directly computed in the JASC algorithm.

2) The total time-averaged expected queue lengths meet the following upper bound:

$$\lim_{T\to\infty} \frac{1}{T} \sum_{\tau=0}^{T-1} \sum_{i\in\mathscr{I}_{entry}\cup\mathscr{I}} \sum_{j\in\mathscr{O}_i} E\left\{f_{ij}(\tau)\right\} \le \frac{3MK^2 + 4\varkappa}{2\ell} + \frac{4\kappa + V\sum_{i\in\mathscr{I}_{entry}} \sum_{j\in\mathscr{O}_i} \sum_{m\in\mathscr{M}} \hbar_{ij}\bar{a}_i^{m*} g_{ij}}{2\ell} \tag{19}$$

where ℓ represents a parameter within the bounds 0 to $\ell_{\max}$ and scales with reserve capacity.

3) The queue length $f_{ij}(\tau)$ at the entry link $i \in \mathscr{I}_{entry}$ for all τ satisfies:

$$f_{ij}(\tau) \le \frac{V\hbar_{ij}}{2} + 2|\hat{\omega}| + a_{ij}^M \tag{20}$$

where $|\hat{\omega}|$ represents the absolute value of $\hat{\omega}$.

Eq. (18) shows that network throughput can approach its maximum if the control parameter V is large enough, making $\frac{3MK^2+4\varkappa+4\kappa}{V}$ negligible. Conversely, Eq. (19) indicates that mean queue lengths increase linearly with V, implying a proportional rise in average delay. This creates a $[O(1/V), O(V)]$ throughput-delay trade-off. From this trade-off, we can deduce that if link queue capacity is unconstrained, a large V allows network throughput to nearly reach its maximum. This shows that JASC can achieve throughput performance similar to MP signal control from [20]. The terms $\varkappa$ and κ in Eqs. (18) and (19) reflect the impacts of queue length estimation errors. These errors increase average queue lengths and reduce network throughput. According to Little's theorem, this directly results in higher average delay, which aligns with expectations. The estimation of mean turn ratios is based on an exponential averaging scheme (see Eq. (12)), which ensures that $\widetilde{G}_{ij}(\tau)$ remains an unbiased estimator of the true mean turn ratio

g_{ij} when the queueing process is positive recurrent [34]. As reflected in Eq. (A-6) of the Supplementary Materials, the expectation of turn ratio estimation errors vanishes in the Lyapunov drift analysis. Therefore, from the perspective of stochastic queue evolution, turn ratio estimation errors do not alter the expected drift or steady-state queue dynamics. Consequently, they do not lead to any degradation in either network throughput or average delay.

Eqs. (18) and (19) show that increasing V reduces the impact of queue length estimation error $\hat{\omega}$ on both throughput and delay, with a more significant effect on the former. For example, increasing V from 2 to 40 reduces the impact of queue length estimation errors on throughput by 20 times. Eq. (19) also indicates that increasing V lowers the weight of queue length estimation errors on the upper bound of average queue length, thereby diminishing their effect on average delay. This impact on average delay depends on the size of the optimal input rate and its proximity to the capacity region boundary. Additionally, parameter ℓ in Eq. (19) correlates with the network reserve capacity. When the input rate approaches the capacity region boundary (i.e., $\ell_{\max}$ approaches zero), the average expected queue lengths tend to increase. This occurs because vehicle arrival rates at intersections nearly match processing rates, resulting in longer queues and, consequently higher average delay, as explained by Little's theorem.

Eq. (20) shows that queues on entry links $i \in \mathscr{I}_{entry}$ consistently remain within bounds. We define $\vec{\Theta} = \{\Theta_i, i \in \mathscr{I}_{entry}\}$, where $\Theta_i = \max_{j \in \mathscr{O}_i} \left[\frac{V\hbar_{ij}}{2} + 2|\hat{\omega}| + a_{ij}^M\right]$. Using the routing matrix $\mathbf{H}$ from Proposition 2, we define $\vec{\mho} = \vec{\Theta}\mathbf{H}$, where $\vec{\mho} = \{\mho_i, i \in \mathscr{I}_{all}\}$. With a known $\mathbf{H}$, the vector $\vec{\mho}$ helps determine the maximum real-time queue length for each link. If the lengths of all links $i \in \mathscr{I}_{all}$ are greater than $\mho_i$, the JASC algorithm can maintain consistent throughput and delay performance. In a network with short links, adjusting V ensures queue lengths stay within queue capacity, preventing congestion spillbacks. This allows lower bounds on throughput and upper limits on average queue lengths to be derived from Eqs. (18) and (19). For the intersection in Fig. 4, if lane 1 is short, setting V no greater than $\frac{2\varrho - 4|\hat{\omega}| - 2a_{13}^M}{\hbar_{13}}$ ensures that queue $f_{13}(\tau)$ does not exceed the physical length ϱ of lane 1. Using Eq. (18), the maximum lower bound on throughput is calculated as $-\frac{(3MK^2+4\varkappa+4\kappa)\hbar_{13}}{2\varrho-4|\hat{\omega}|-2a_{13}^M} + \sum_{m\in\mathscr{M}} \hbar_{13}\bar{a}_1^{m*} + \sum_{m\in\mathscr{M}} \hbar_{42}\bar{a}_4^{m*}$, considering that $g_{13} = g_{42} = 1$.

Remark 2: The vector $\vec{\mho}$ specifies the maximum real-time queue lengths for all links, which is not previously addressed in MP signal control literature. Prior research assumed infinite queue capacity and only provided upper bounds for total average expected queue lengths to guarantee network stability in mean. Varaiya [20] stated that finite queue capacity is incompatible with MP signal control, as it cannot guarantee bounded average queue lengths, potentially causing network congestion. In contrast, admission control regulates inflows at entry links, ensuring real-time queue lengths remain within set bounds. By fine-tuning V, the JASC algorithm keeps queue lengths below the finite queue capacity threshold, preserving network stability and preventing overflows. Furthermore, with a carefully chosen V, the JASC algorithm specifies the highest average delay and the lowest achievable network throughput, considering finite queue capacity. In this study, queue lengths are quantified by the number of vehicles rather than physical distance. Accordingly, the "queue capacity" discussed here should be interpreted as the maximum number of vehicles that can be accommodated on a link when all vehicles maintain their minimum safe spacing. The network structure is highly complex, and accurately determining the optimal value of V is generally difficult. In practice, an empirical upper bound of V can be estimated based on the congestion density of the shortest link, which is typically the most constrained link in the network, together with the queue upper bounds $\vec{\Theta}$ at the entry links. Specifically, V should be chosen such that the maximum queue lengths remain below $\vec{\Theta}$ under recurrent demand conditions, thereby preventing network oversaturation and queue overflow. A larger V typically prioritizes throughput at the expense of increased delay, whereas a smaller V emphasizes delay minimization but may reduce overall throughput. Therefore, V can be gradually tuned within this empirically estimated range until a satisfactory trade-off between throughput and delay is achieved for the given network configuration.

C. Performance Analysis

We construct a Lyapunov drift optimization function to validate Theorem 2:

$$\Delta(\mathbf{F}(\tau)) - V\sum_{i\in\mathscr{I}_{entry}}\sum_{j\in\mathscr{O}_i}\sum_{m\in\mathscr{M}}\hbar_{ij}E\left\{a_{ij}^m(\tau+1)\middle|\mathbf{F}(\tau)\right\} \tag{21}$$

where $\Delta(\mathbf{F}(\tau)) \triangleq E\{L(\mathbf{F}(\tau+1)) - L(\mathbf{F}(\tau))|\mathbf{F}(\tau)\}$ measures the expected change in the sum of squared queue lengths $L(\mathbf{F}(\tau))$ (i.e., $L(\mathbf{F}(\tau)) = \sum_{i\in\mathscr{I}_{entry}\cup\mathscr{I}}\sum_{j\in\mathscr{O}_i} f_{ij}^2(\tau)$) from one period to another. This Lyapunov drift function $\Delta(\mathbf{F}(\tau))$ is crucial for proving strong queue stability and is widely used in research such as [20] and [29]. The principle is straightforward: a lower $L(\mathbf{F}(\tau))$ implies shorter queues, while a higher value indicates at least one long queue. Actively minimizing $\Delta(\mathbf{F}(\tau))$ moves the network towards lower congestion, inherently stabilizing it. However, focusing solely on minimizing $\Delta(\mathbf{F}(\tau))$ can overly restrict inflows and lower throughput. Introducing a positive parameter V allows for a balanced tradeoff between congestion mitigation and throughput maximization. This parameter enables the function to manage the trade-off effectively, ensuring that the network maintains stability while maintaining high throughput.

Lemma 1: For any τ, JASC guarantees the following upper bound for Eq. (21):

$$\begin{aligned}
&\Delta(\mathbf{F}(\tau)) - V\sum_{i\in\mathscr{I}_{entry}}\sum_{j\in\mathscr{O}_i}\sum_{m\in\mathscr{M}}\hbar_{ij}E\left\{a_{ij}^m(\tau+1)\middle|\mathbf{F}(\tau)\right\} \leq \\
&\quad -2\sum_{i\in\mathscr{I}_{entry}\cup\mathscr{I}}\sum_{j\in\mathscr{O}_i}E\left\{p_{ij}w_{ij}\left(\tilde{\mathbf{F}}(\tau)\right)X_{ij}(\tau)\middle|\mathbf{F}(\tau)\right\} + 2\varkappa \\
&\quad + 3MK^2 + \sum_{i\in\mathscr{I}_{entry}}\sum_{j\in\mathscr{O}_i}\sum_{m\in\mathscr{M}}\left(2\tilde{f}_{ij}(\tau) - V\hbar_{ij} + 2\hat{\omega}\right) \\
&\quad \times E\left\{a_{ij}^m(\tau+1)\middle|\mathbf{F}(\tau)\right\}
\end{aligned} \tag{22}$$

where parameters $\varkappa$, K, and M are specified in Eq. (18), while $\hat{\omega}$ is defined in Eq. (13).

Proof: For a detailed proof, refer to Appendix A in the supplementary material. ■

Remark 3: The fundamental design principle of JASC draws from the structure of Eq. (22). Signal control focuses on minimizing the first term of the upper bound, while admission control concentrates on reducing the fourth term. Such a division of tasks allows JASC to balance maximizing network throughput and minimizing congestion. This balance is achieved by specifically minimizing the upper bound of Eq. (21). Therefore, JASC effectively improves overall network performance by simultaneously reducing congestion and increasing throughput.

We further simplify Lemma 1 to support the proof of Theorem 2.

Lemma 2: For any τ, JASC guarantees:

$$\begin{aligned}&\Delta(\mathbf{F}(\tau)) - V\sum_{i\in\mathscr{I}_{entry}}\sum_{j\in\mathscr{O}_i}\sum_{m\in\mathscr{M}}\hbar_{ij}E\left\{a_{ij}^m(\tau+1)\middle|\mathbf{F}(\tau)\right\}\\&\le 3MK^2+4\varkappa+4\kappa-2\ell|\mathbf{F}(\tau)|\\&\quad - V\sum_{i\in\mathscr{I}_{entry}}\sum_{j\in\mathscr{O}_i}\sum_{m\in\mathscr{M}}\hbar_{ij}\bar{a}_i^{m*}g_{ij}\end{aligned}\tag{23}$$

where the parameter ℓ is described in Proposition 3. The term $|\mathbf{F}(\tau)|$, representing the total length of intersection queues during period τ, is calculated as $\sum_{i\in\mathscr{I}_{entry}\cup\mathscr{I}}\sum_{j\in\mathscr{O}_i}f_{ij}(\tau)$.

Proof: The detailed proof is available in Appendix B in the supplementary material. ■

Based on Lemma 2, the proof of Theorem 2 is as follows. Taking the expected value of Eq. (23) over $\mathbf{F}(\tau)$ results in:

$$\begin{aligned}&E\{L(\mathbf{F}(\tau+1))\}-E\{L(\mathbf{F}(\tau))\}\\&\quad - V\sum_{i\in\mathscr{I}_{entry}}\sum_{j\in\mathscr{O}_i}\sum_{m\in\mathscr{M}}\hbar_{ij}E\left\{a_{ij}^m(\tau+1)\right\}\\&\le 3MK^2+4\varkappa+4\kappa-2\ell\sum_{i\in\mathscr{I}_{entry}\cup\mathscr{I}}\sum_{j\in\mathscr{O}_i}E\left\{f_{ij}(\tau)\right\}\\&\quad - V\sum_{i\in\mathscr{I}_{entry}}\sum_{j\in\mathscr{O}_i}\sum_{m\in\mathscr{M}}\hbar_{ij}\bar{a}_i^{m*}g_{ij}\end{aligned}\tag{24}$$

Calculating the sum of the aforementioned inequality across all τ within the range $\{0,\ldots,T-1\}$ results in:

$$\begin{aligned}&E\{L(\mathbf{F}(T))\}-E\{L(\mathbf{F}(0))\}\\&\quad - V\sum_{\tau=1}^{T}\sum_{i\in\mathscr{I}_{entry}}\sum_{j\in\mathscr{O}_i}\sum_{m\in\mathscr{M}}\hbar_{ij}E\left\{a_{ij}^m(\tau)\right\}\\&\le \left(3MK^2+4\varkappa+4\kappa\right)T-2\ell\sum_{\tau=0}^{T-1}\sum_{i\in\mathscr{I}_{entry}\cup\mathscr{I}}\sum_{j\in\mathscr{O}_i}E\left\{f_{ij}(\tau)\right\}\\&\quad - VT\sum_{i\in\mathscr{I}_{entry}}\sum_{j\in\mathscr{O}_i}\sum_{m\in\mathscr{M}}\hbar_{ij}\bar{a}_i^{m*}g_{ij}\end{aligned}\tag{25}$$

Dividing the given inequality by $-TV$ and then considering the limit as T tends towards infinity result in:

$$\begin{aligned}&\lim_{T\to\infty}\frac{1}{T}\sum_{\tau=1}^{T}\sum_{i\in\mathscr{I}_{entry}}\sum_{j\in\mathscr{O}_i}\sum_{m\in\mathscr{M}}\hbar_{ij}E\left\{a_{ij}^m(\tau)\right\}\\&\ge -\frac{3MK^2+4\varkappa+4\kappa}{V}+\sum_{i\in\mathscr{I}_{entry}}\sum_{j\in\mathscr{O}_i}\sum_{m\in\mathscr{M}}\hbar_{ij}\bar{a}_i^{m*}g_{ij}\end{aligned}\tag{26}$$

The proof of result 1 of Theorem 2 ends.

To prove the result 2 of Theorem 2, Eq. (25) is rewritten as follows:

$$\begin{aligned}&2\ell\sum_{\tau=0}^{T-1}\sum_{i\in\mathscr{I}_{entry}\cup\mathscr{I}}\sum_{j\in\mathscr{O}_i}E\left\{f_{ij}(\tau)\right\}\\&\le E\{L(\mathbf{F}(0))\}+V\sum_{\tau=1}^{T}\sum_{i\in\mathscr{I}_{entry}}\sum_{j\in\mathscr{O}_i}\sum_{m\in\mathscr{M}}\hbar_{ij}E\left\{a_{ij}^m(\tau)\right\}\\&\quad+\left(3MK^2+4\varkappa+4\kappa\right)T\end{aligned}\tag{27}$$

Dividing Eq. (27) by $2T\epsilon$ and subsequently taking the limit as T approaches infinity lead to:

$$\begin{aligned}&\lim_{T\to\infty}\frac{1}{T}\sum_{\tau=0}^{T-1}\sum_{i\in\mathscr{I}_{entry}\cup\mathscr{I}}\sum_{j\in\mathscr{O}_i}E\left\{f_{ij}(\tau)\right\}\\&\le\frac{3MK^2+4\varkappa+4\kappa+V\sum_{i\in\mathscr{I}_{entry}}\sum_{j\in\mathscr{O}_i}\sum_{m\in\mathscr{M}}\hbar_{ij}\bar{a}_{ij}^m}{2\ell}\\&\le\frac{3MK^2+4\varkappa+4\kappa+V\sum_{i\in\mathscr{I}_{entry}}\sum_{j\in\mathscr{O}_i}\sum_{m\in\mathscr{M}}\hbar_{ij}\bar{a}_i^{m*}g_{ij}}{2\ell}\end{aligned}\tag{28}$$

The above first inequality utilizes the definition of $\bar{a}_{ij}^m = \lim_{T\to\infty}\frac{1}{T}\sum_{\tau=0}^{T-1}E\left\{a_{ij}^m(\tau)\right\}$. The second inequality above holds because $\sum_{i\in\mathscr{I}_{entry}}\sum_{j\in\mathscr{O}_i}\sum_{m\in\mathscr{M}}\hbar_{ij}\bar{a}_i^{m*}g_{ij}$ is the maximum network throughput defined in Eq. (18). The proof of result 2 of Theorem 2 ends.

Under admission control guidelines, up to a_{ij}^M vehicles are allowed to enter the queue $f_{ij}(\tau)$ on the entry link $i\in\mathscr{I}_{entry}$, if $\tilde{f}_{ij}(\tau)$ does not exceed $\frac{V\hbar_{ij}-2\hat{\omega}}{2}$. If this threshold is surpassed, no additional vehicles join the queue. As a result, following these admission control measures and Eq. (11), it is ensured that $f_{ij}(\tau)$ remains at or below $\frac{V\hbar_{ij}}{2}+2|\hat{\omega}|+a_{ij}^M$. The proof of result 3 of Theorem 2 ends. ■

V. Numerical Simulation

Section V-A demonstrates the effectiveness of the performance analysis of JASC using an isolated intersection. In Section V-B, we compare the proposed JASC algorithm with published algorithms through simulations on a real signalized network to highlight its advantages. All simulations are conducted using the microscopic simulation tool SUMO.

A. Isolated Intersection Experiment

We validate Theorem 2 using the simplified intersection in Fig. 4. Phases 1 and 2 can be represented as turns (4,2) and (1,3), respectively. Following [25], each period has a fixed duration of 5 seconds, saturation flow rates p_{13} and p_{42} are 2.5 vehicles per period (veh/slot), and saturation input rates a_{13}^M and a_{42}^M are also 2.5 veh/slot. Each lane is 200 meters long. For traffic-state reconstruction, each lane is discretized into cells of length D_{ij}^c = 10 m (i.e., 20 cells per 200 m lane). CVs transmit speed information every 5 seconds. The kernel function in Eq. (7) uses spatial and temporal parameters ψ = 20 m and

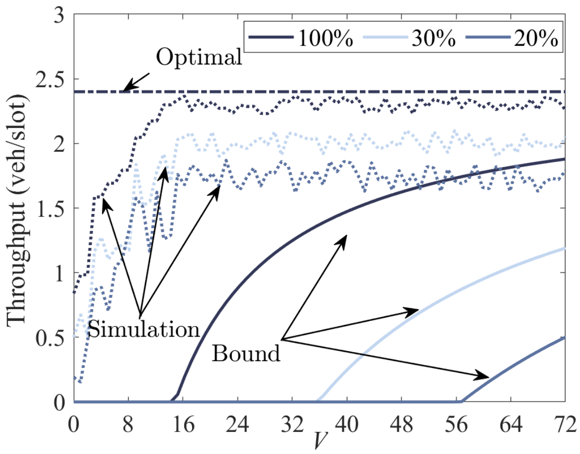

Fig. 5. Intersection throughput under different CV penetration rates.

$\iota = 5$ s based on [39] and [52]. According to [39], parameters shockwave speed υ_{ij}, congestion density ρ_{ij}^{jam}, and free flow speed v_{ij}^{free} are set to 25 km/h, 143 veh/km, and 60 km/h, respectively. Vehicles exit the intersection when they reach the end nodes of lanes 2 and 3, so queues exist only on lanes 1 and 4. We set asymmetric arrival rates $\bar{a}_1 = 1.7$ veh/slot and $\bar{a}_4 = 0.7$ veh/slot. The arrival rate for each lane is the sum of the arrival rates of CVs and RVs. The type of arriving vehicles is determined randomly based on the corresponding CV penetration rate. Since there are only two traffic flows ($1 \rightarrow 3$ and $4 \rightarrow 2$), the arrival rates of turns (1,3) and (4,2) are $\sum_{m\in\mathscr{M}} \bar{a}_{13}^m = \bar{a}_1 = 1.7$ veh/slot and $\sum_{m\in\mathscr{M}} \bar{a}_{42}^m = \bar{a}_4 = 0.7$ veh/slot. Random turn rates $G_{13}(\tau)$ and $G_{42}(\tau)$ are both 1 at any period τ. Based on Proposition 3, the arrival rates fall inside the capacity region, with $\ell_{\max}$ measuring a distance of 0.05 from the boundary. The weights $\hbar_{13}$ and $\hbar_{42}$ of input rates $\sum_{m\in\mathscr{M}} \bar{a}_{13}^m$ and $\sum_{m\in\mathscr{M}} \bar{a}_{42}^m$ are set to 1.

To accurately determine the upper bound of queue lengths and the lower bound of intersection throughput, it is necessary to specify the queue length estimation error upper bound $\hat{\omega}$. A periodic phase pattern is applied, where turning movements (1,3) and (4,2) are executed alternately at every period. We evaluate the queue length estimator in Section IV-A at CV penetration rates of 10%, 20%, and 30%. The 95% absolute error bands are within ± 3, ± 2, and ± 1 vehicles for the 10%, 20%, and 30% penetration scenarios, respectively, corresponding to approximately 27%, 18%, and 9% of the per-lane storage capacity (about 11 vehicles). The upper bounds of estimation errors do not exceed 4, 3, and 2 vehicles under these three penetration levels, respectively, which are used as the values of $\hat{\omega}$ in the subsequent simulations.

After obtaining the maximum queue length estimation error $\hat{\omega}$ under each CV penetration rate, the lower bound on intersection throughput, the upper limit for total time-averaged expected queue lengths, and real-time queue length bounds for $f_{13}(\tau)$ and $f_{42}(\tau)$ can be determined by Eqs. (18)–(20), respectively. Based on the above simulation settings, parameters M, κ, and $\varkappa$ are 2, $2.4\hat{\omega}$, and $10\hat{\omega}$, respectively. Since the arrival rates are feasible, the optimal throughput is equal to 2.4 veh/slot (i.e., $\sum_{m\in\mathscr{M}} \bar{a}_{13}^m + \sum_{m\in\mathscr{M}} \bar{a}_{42}^m = 2.4$ veh/slot). We calculate the optimal throughput to demonstrate the validity of the theoretical bounds in Theorem 2. There is no need to utilize optimal throughput in numerical simulations. According to [57], one vehicle occupies a five-meter space. This 200-meter lane can be occupied by up to 40 vehicles, which means that both real-time queue lengths $f_{13}(\tau)$ and $f_{42}(\tau)$ should be less than 40 vehicles. According to the queue length estimation under 20% CV penetration rate, the maximum queue length estimation error $\hat{\omega}$ is 3. From Eq. (20), we know that parameter V should not exceed 72 where $\hat{\omega}$ takes the value 3. Therefore, we vary V from 1 to 72 in 1 interval to perform simulations. Each simulation takes 2880 periods (i.e., 4 hours). We perform simulations at CV penetration rates of 20%, 30%, and 100%. To avoid the simulation results being affected by the initial perturbation, the simulation results of the first hour are removed.

Fig. 5 shows intersection throughput simulation results, illustrating that it gradually approaches the optimal value as V increases. As CV penetration rates increase, the maximum queue length estimation error $\hat{\omega}$ decreases, and intersection throughput decreases according to Eq. (18). The simulation results in Fig. 5 also verify this. According to Eq. (19), we know that real-time queue length bounds are low, with small V. Therefore, we show the simulation results of real-time queue lengths $f_{13}(\tau)$ and $f_{42}(\tau)$ at V from 10 to 20 under the 30% CV penetration rate in the form of boxplots in Fig. 6. In Fig. 6, real-time queue length bounds are determined by Eq. (20). Fig. 6 shows that both real-time queue lengths $f_{13}(\tau)$ and $f_{42}(\tau)$ are smaller than the upper bounds. Therefore, the developed admission control algorithm effectively manages real-time queue length upper bounds. Fig. 6 also demonstrates that the mean queue length on each lane increases as V increases. Thus, from the results of Figs. 5 and 6, it is clear that JASC provides an effective tradeoff between throughput and delay.

B. Network Experiments

This section validates JASC through comparative simulations on a network from Gothenburg, Sweden (see Fig. 7). The parameter settings related to queue length estimation are consistent with those used in the isolated intersection experiments. The network consists of 16 intersections and 80 one-way links, with 16 entry links and 16 exit links. All intersections adopt the four-phase mechanism shown in Fig. 8. Each link has three distinct lanes for straight travel, left turns, and right turns. MP and actuated control (AC) are introduced as comparison algorithms. The MP algorithm from [20] converts the estimated queue lengths and turn ratios in the signal control algorithm in Section IV-B into accurate values. The AC uses detector input to decide whether to extend the current green phase or switch to another phase. If vehicles are detected in the approach lanes, the green phase can be extended by a set time increment until the maximum green time is reached. To demonstrate how parameter V balances delay and throughput, we vary V in JASC to 2, 5, 10, 20, and 30, labeled JASC-V2, JASC-V5, JASC-V10, JASC-V20, and JASC-V30. Network throughput is assessed under phase update intervals of 15, 20, 25, 30, and 35 seconds. The highest

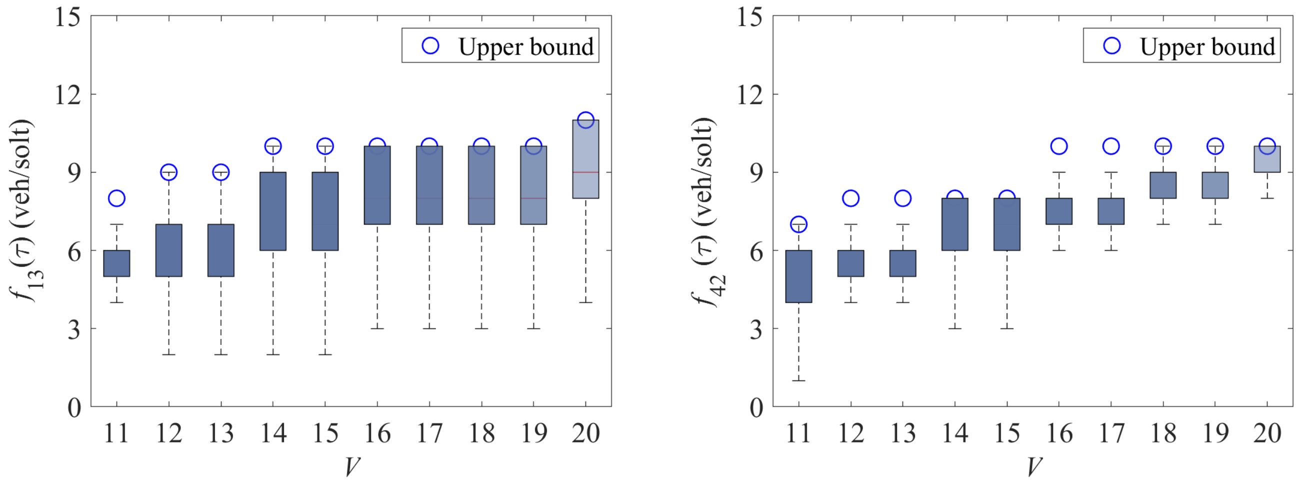

(a) $f_{13}(\tau)$ (b) $f_{42}(\tau)$

Fig. 6. Queue length boxplots under the 30% CV penetration rate.

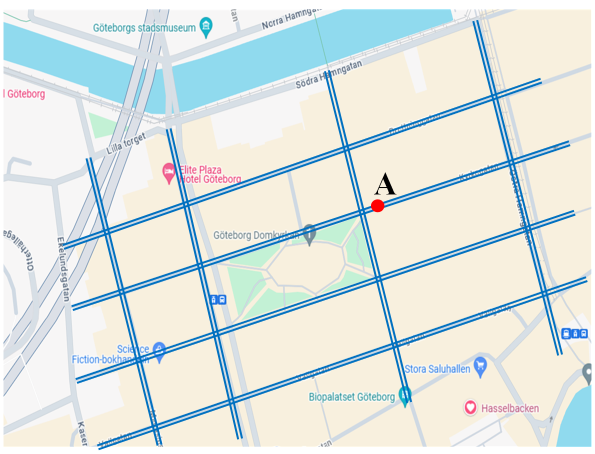

Fig. 7. Network from gothenburg, Sweden.

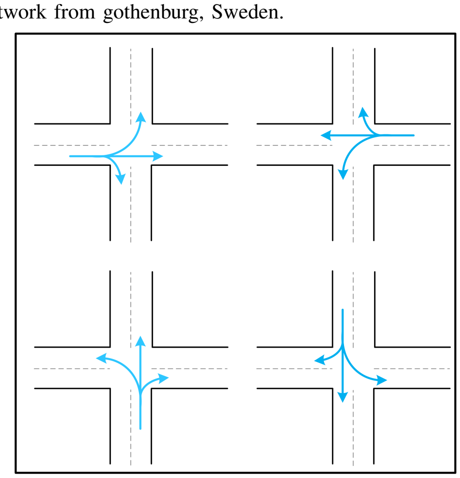

Fig. 8. Candidate signal phases.

network throughput occurs at 20 and 25 seconds, with 20 seconds providing the most robust performance. Therefore, all algorithms update signal phases every 20 seconds. Following [34], smoothing factor λ is set to 0.02.

1) Capacity Region: Following [41], we establish the capacity region boundary by applying uniform demand at entry nodes. Comparative simulations are conducted by varying demand from 200 to 1250 vehicles per hour (veh/h) in 50-veh/h increments. For the JASC algorithm, network performance is tested under CV penetration rates of 10%, 20%, 30%, and 100%. The 100% CV penetration rate serves as a benchmark, representing the outcome of JASC with accurate queue length information and mean turn ratios. Each simulation runs for three hours. The average computation times of the JASC algorithm, obtained by averaging over all control parameters ($V = 2, 5, 10, 20$, and 30), increase moderately with the demand level. Specifically, the average times are approximately 52.9, 62.8, 76.1, 94.1, 115.5, 131.6, 173.1, 215.5, 261.0, 333.8, and 376.9 seconds for demand levels of 200, 300, 400, 500, 600, 700, 800, 900, 1000, 1100, and 1200 veh/h, respectively. These results indicate that the computational cost grows gradually with demand but remains well within real-time simulation capability, confirming the scalability of the proposed JASC framework. Fig. 9 shows average trip delay and network throughput, where the black curves correspond to the average trip delay on the left axis, and the dark blue curves correspond to the throughput on the right axis. Under the AC algorithm, the maximum network throughput fluctuates near 9760 veh/h for demand ranging from 600 veh/h to 900 veh/h. Network throughput reaches its maximum under the MP control algorithm at a demand of 700 veh/h, amounting to 11245 veh/h. When demand exceeds the critical node/range, both AC and MP experience significant increases in trip delay and sharp drops in throughput. Hence, a demand of 700 veh/h can be defined as the capacity region boundary under the MP control algorithm. Fig. 9(a) also shows that when demand exceeds the critical point, the average trip delay and throughput performance of the MP algorithm is worse than that of AC. This further verifies the results of [20], that MP performs poorly in networks with limited queue capacity and is only suitable for demands within the capacity region. However, under the JASC algorithm, network throughput increases with demand and shows only minor fluctuations after reaching its peak. This indicates that the admission control in JASC effectively prevents network oversaturation.

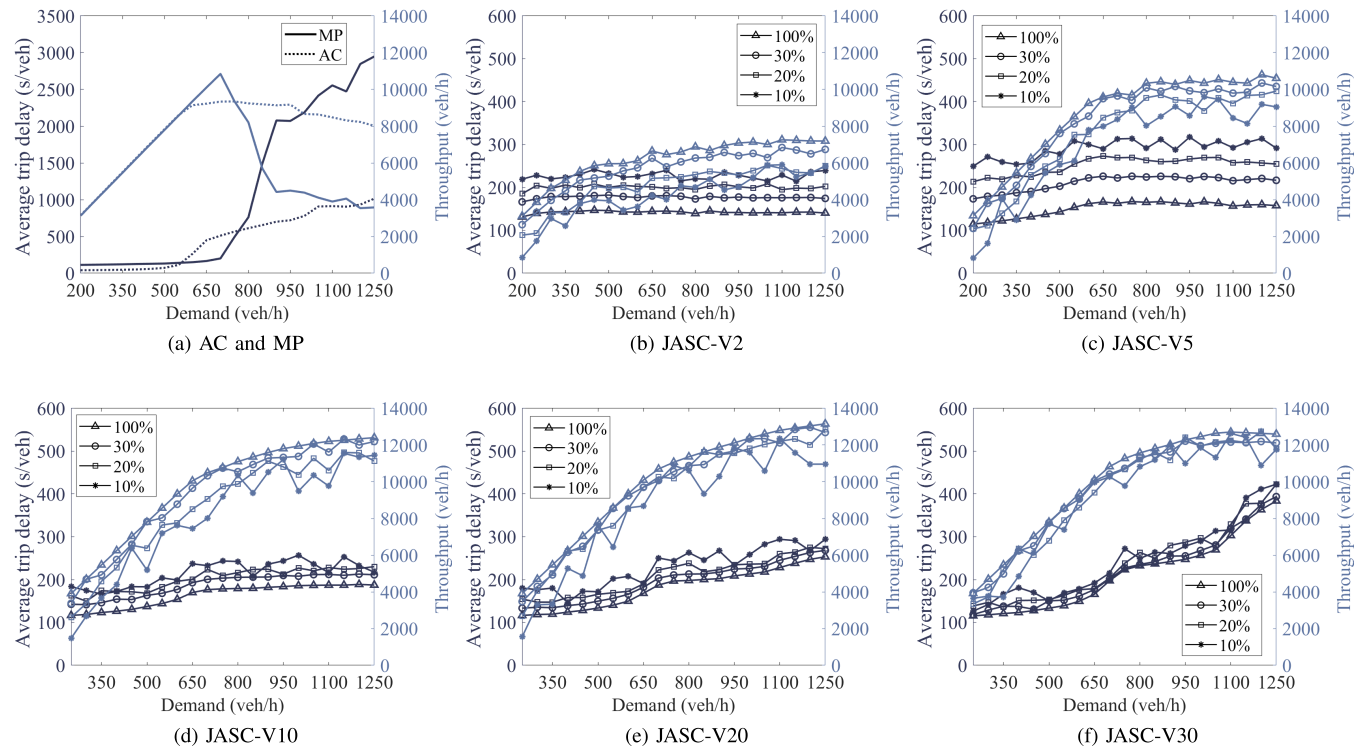

Fig. 9. The basic simulation results.

At demand levels below 550 veh/h, AC results in an average trip delay that is half of that observed with MP and JASC. Compared to AC, the MP algorithm increases maximum throughput by 13.2%. Under JASC-V2, JASC-V5, JASC-V10, JASC-V20, and JASC-V30 algorithms, the maximum throughput at the 100% CV penetration rate is 7045, 11240, 12860, 13440, and 12590 veh/h, respectively. The corresponding average trip delays are 139.7, 155.3, 181.4, 245.0, and 369.4 seconds per vehicle (s/veh). Compared to MP, JASC achieves the largest increase in maximum throughput at $V = 20$, with a 16.3% improvement. Except for $V = 30$, the JASC algorithm gradually increases average trip delay and network throughput with the increase of V, effectively achieving a tradeoff between delay and throughput. When V increases from 20 to 30, the JASC algorithm reduces maximum throughput while increasing average trip delay. This is because the network structure is overly complex, and the maximum V is not estimated based on link lengths and turn ratios. These results indicate that at $V = 30$, admission control allows excessive inflow into the network, causing spillbacks and preventing JASC from balancing throughput and delay.

Figs. 9(b) to 9(f) show that as CV penetration rates increase, both network throughput and delay performances under the JASC algorithm improve. This observation confirms the first two results in Theorem 2. As CV penetration rates increase, the terms $\varkappa$ and κ, which are associated with the queue length estimation error $\hat{\omega}$, decrease, thereby narrowing the gap between throughput and average delay and their respective optimal values. Further observation shows that increasing V reduces the sensitivity of throughput to CV penetration much more than that of average trip delay. This aligns with Theorem 2, as increasing V reduces the influence of $\varkappa$ and κ more strongly for throughput than for average delay. When V is set to 20 and 30, the performance of average trip delay and throughput at a 30% CV penetration rate is nearly the same as at 100%. Combining all the above analyses, $V = 20$ is an effective value, as it reduces average trip delay, achieves high throughput, and maintains good performance even at low CV penetration rates.

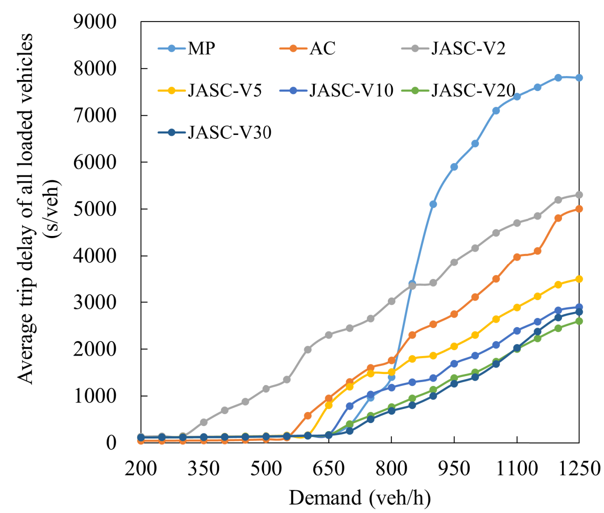

Fig. 10. The completed trip delay of all loaded vehicles.

The admission control in JASC indeed restricts some vehicles from entering the network, thereby increasing their

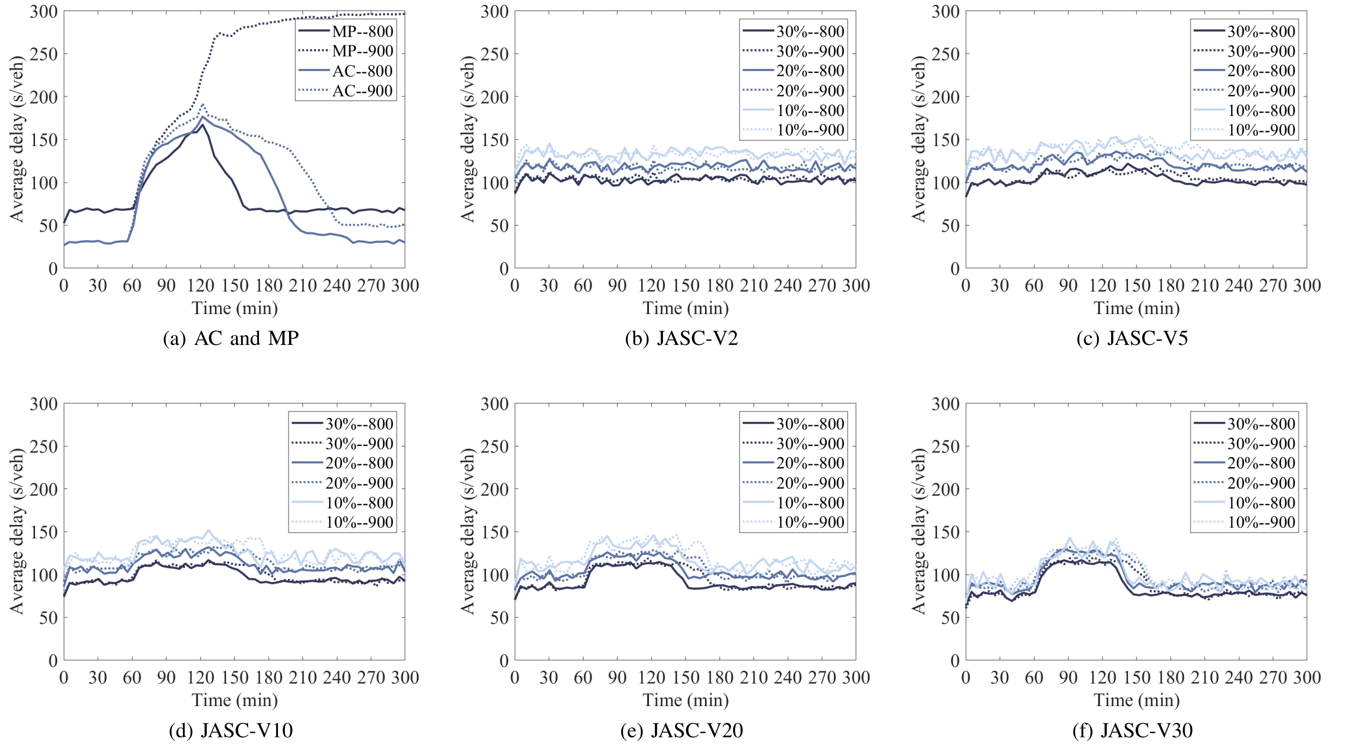

Fig. 11. The simulation results of average delay under sudden demand.

waiting delay to enter and further impacting completed trip delay. However, admission control effectively prevents network oversaturation, maintaining high throughput and thus reducing the delay for vehicles traveling through the network. To further evaluate its impact on trip delay, simulations assess the completed trip delay, including both entry waiting time and travel delay. Previous simulations show that JASC with a 30% CV penetration rate performs similarly to 100% penetration. Thus, we use JASC with a 30% CV penetration rate as an example to evaluate the completed trip delay for all loaded vehicles. The results are shown in Fig. 10.

In Fig. 10, before the network becomes oversaturated (i.e., demand does not exceed 750 veh/h), the MP algorithm, which aims to maximize throughput, shows excellent advantages, causing less trip delay than the AC algorithm and the JASC algorithm with parameter V values of 2, 5, and 10. With small V values, the JASC algorithm overly restricts vehicle entry, resulting in substantial delays in completed trips. In the demand range of 650 to 750 veh/h, the JASC algorithm with V values of 20 and 30 causes less delay than the MP algorithm. As shown in Fig. 9, the JASC algorithm improves capacity and throughput in networks with limited queue capacity. Within this demand range, it effectively regulates input rates to fully utilize network capacity, reducing completed trip delay.

As demand increases, the completed trip delay under the MP algorithm rises significantly, eventually exceeding those observed with the JASC algorithm (for all V values) and the AC algorithm. Thus, under feasible demand, the MP algorithm improves network throughput and reduces delay through intersection coordination. However, under infeasible demand, its performance worsens, even falling below that of the AC algorithm, which focuses on reducing delay at individual intersections. This difference reflects the design goals of the AC and MP algorithms. Additionally, as demand increases, the average delay under the JASC algorithm with any V value also increases but remains lower than that of the MP algorithm. Except for $V = 2$, the JASC algorithm with other V values (especially 20 and 30) performs significantly better than the AC algorithm. This indicates that admission control with an appropriate V effectively avoids network oversaturation and maximizes the advantages of the MP algorithm.

2) Evaluating Adaptability to Bursty Demand: The section examines how JASC performs when faced with sudden changes in demand. As established earlier, the capacity region boundary under MP is 700 veh/h. Therefore, we set up two scenarios. Each simulation lasts five hours. In the first scenario, demand rises to 800 veh/h during the second hour and then drops to 400 veh/h for the remaining time. In the second scenario, demand rises to 900 veh/h during the second hour, while the rest of the timeline matching Scenario 1. For the JASC algorithm, simulations are conducted under 10%, 20%, and 30% CV penetration rates. The average delay is tracked every 300 seconds to illustrate current network congestion levels. A 300 s/veh average delay signifies a completely blocked network. Fig. 11 displays simulation results.

The AC algorithm, designed to reduce queue delay, performs well both before and after sudden demand changes. It achieves an average delay of approximately 40 s/veh, which is half that of JASC and MP (around 80 s/veh). After the sudden demand, the AC algorithm restores the average delay

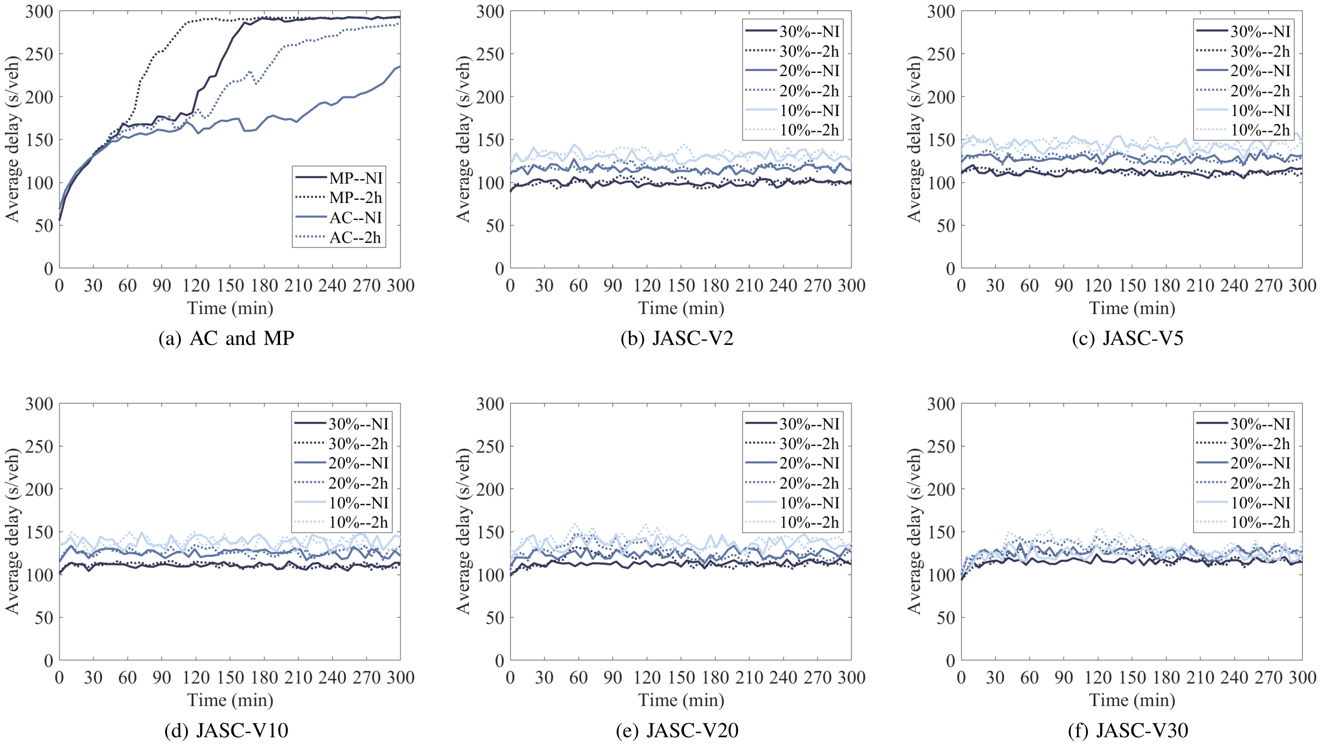

(a) AC and MP (b) JASC-V2 (c) JASC-V5

(d) JASC-V10 (e) JASC-V20 (f) JASC-V30

Fig. 12. Average delay under traffic incidents.

to 80 s/veh in 80 minutes in the first scenario and in 120 minutes in the second scenario. In the first scenario, the MP algorithm takes 50 minutes to normalize the average delay. However, in the second scenario, despite taking 180 minutes, it is unable to restore the average delay to its normal state. The JASC algorithm, with V set to 2 or 5, maintains the average delay nearly unaffected by the sudden demand increase in both scenarios. With parameter V set to 10, 20, or 30, the JASC algorithm restores normal delay within 40 minutes in the first scenario and 75 minutes in the second scenario. These results further highlight that the MP and JASC algorithms, designed to maximize network throughput, quickly recover the average delay by increasing trip completion rates. Comparing Figs. 11(b) to 11(f), as V increases, the impact of CV penetration rates on average delay decreases, further validating the analytical finding of the average delay in Result 2 of Theorem 2.

3) Evaluating Adaptability to Traffic Incidents: The section examines how JASC performs during unexpected traffic incidents. An accident is assumed to occur at point A in Fig. 7, blocking both the straight and left-turn lanes from the 0.5th to the 2.5th hour. The demand is maintained at 800 veh/h throughout each five-hour simulation. Similar to the previous section, numerical simulations are conducted at 10%, 20%, and 30% CV penetration rates, with average delay recorded every 300 seconds. Fig. 12 displays test results, where curves labeled "2h" represent simulations with the two-hour incident, and those labeled "NI" represent simulations with no incident. The results show that the AC and MP algorithms are unable to restore average delay to normal levels even 150 minutes after the incident ends. During the two-hour incident, average delay increases significantly, reaching up to 75 s/veh under AC and 85 s/veh under MP, within 80th and 30th minutes. However, average delay under the JASC algorithm is almost unaffected, especially when V is set to 2, 5, or 10. With V set to 20 or 30, the JASC algorithm causes an increase in average delay of less than 10 s/veh and 20 s/veh, respectively, and normalizes immediately after the incident ends. Therefore, JASC effectively mitigates the impact of sudden incidents on average delay. The influence of CV penetration rates on average delay is similar to that observed in the previous section. When V increases, the impact of queue length estimation errors on average delay at low CV penetration rates decreases. With higher CV penetration rates, average delay further decreases.

VI. CONCLUSION

This study develops and validates an innovative joint admission and signal control algorithm tailored for mixed traffic environments with both CVs and RVs. The proposed algorithm addresses the limitations of traditional MP control strategies by dynamically adjusting input rates and signal phases, ensuring efficient utilization of network capacity while preventing oversaturation. To enhance practical applicability, the algorithm incorporates queue length and mean turn ratio estimation methods, utilizing limited feedback from CVs to estimate mixed queue lengths and mean turn rates. By leveraging a Lyapunov drift optimization function, the JASC algorithm achieves a $[O(1/V), O(V)]$ tradeoff between throughput and delay, adaptable to varying arrival rates and network conditions. Additionally, our analysis quantifies the degradation in network performance due to queue length estimation errors. Extensive simulations across diverse traffic scenarios demonstrate the effectiveness of the JASC algorithm. Results show significant improvements in traffic efficiency, including a 16.3% increase in network throughput and reduced average delays, particularly in high-demand urban settings. Furthermore, the algorithm's flexibility and scalability ensure its applicability in modern traffic systems, effectively managing congestion and enhancing network resilience under dynamic and unpredictable conditions.

In future work, we will explore two main research directions. First, we aim to guide CVs toward more efficient route choices to better utilize network capacity and alleviate congestion. Second, we plan to distinguish between queued and non-queued vehicles on long links, enabling more effective use of intersection resources and improving overall traffic flow efficiency.

References

[1] Q. Ji, X. Wen, J. Jin, Y. Zhu, and Y. Lv, "Urban traffic control meets decision recommendation system: A survey and perspective," *IEEE/CAA J. Autom. Sinica*, vol. 11, no. 10, pp. 2043–2058, Oct. 2024.

[2] Y. Shi, Z. Wang, T. J. LaClair, C. Wang, Y. Shao, and J. Yuan, "A novel deep reinforcement learning approach to traffic signal control with connected vehicles," *Appl. Sci.*, vol. 13, no. 4, p. 2750, Feb. 2023.

[3] X. Liang, S. I. Guler, and V. V. Gayah, "An equitable traffic signal control scheme at isolated signalized intersections using connected vehicle technology," *Transp. Res. C, Emerg. Technol.*, vol. 110, pp. 81–97, Jan. 2020.

[4] Q. Guo and X. Ban, "Network multiscale urban traffic control with mixed traffic flow," *Transp. Res. B, Methodol.*, vol. 185, Jul. 2024, Art. no. 102963.

[5] N. Gupta, G. R. Patil, and H. L. Vu, "Efficacy of decentralized traffic signal controllers on stabilizing heterogeneous urban grid network," *Commun. Transp. Res.*, vol. 4, Dec. 2024, Art. no. 100137.

[6] X. Chen, X. Lin, M. Li, F. He, and Q. Meng, "A nearly throughput-maximum knotted intersection design and control for connected and automated vehicles," *Transp. Res. B, Methodol.*, vol. 171, pp. 44–79, May 2023.

[7] S. Liao, Y. Wu, K. Ma, and Y. Niu, "Ant colony optimization with look-ahead mechanism for dynamic traffic signal control of IoV systems," *IEEE Internet Things J.*, vol. 11, no. 1, pp. 366–377, Jan. 2024.

[8] Y. Zhu, Y. Lv, S. Lin, and J. Xu, "A stochastic traffic flow model-based reinforcement learning framework for advanced traffic signal control," *IEEE Trans. Intell. Transp. Syst.*, vol. 26, no. 1, pp. 714–723, Jan. 2025.

[9] Y. Bie, Y. Ji, and D. Ma, "Multi-agent deep reinforcement learning collaborative traffic signal control method considering intersection heterogeneity," *Transp. Res. C, Emerg. Technol.*, vol. 164, Jul. 2024, Art. no. 104663.

[10] Y. Tang, X. Dai, and Y. Lv, "Large language model-assisted arterial traffic signal control," *IEEE J. Radio Freq. Identificat.*, vol. 8, pp. 322–326, 2024.

[11] N. Gupta, G. R. Patil, and H. L. Vu, "Simple abstract models to study stability of urban networks with decentralized signal control," *Transp. Res. B, Methodol.*, vol. 172, pp. 93–116, Jun. 2023.

[12] Z. Hao and R. Boel, "Convergence analysis on control for traffic signals in urban road network," *Transp. Res. B, Methodol.*, vol. 165, pp. 35–62, Nov. 2022.

[13] Z. Hao, R. Boel, and Z. Li, "Model based urban traffic control, part I: Local model and local model predictive controllers," *Transp. Res. C, Emerg. Technol.*, vol. 97, pp. 61–81, Dec. 2018.

[14] Z. Mo, W. Li, Y. Fu, K. Ruan, and X. Di, "CVLight: Decentralized learning for adaptive traffic signal control with connected vehicles," *Transp. Res. C, Emerg. Technol.*, vol. 141, Aug. 2022, Art. no. 103728.

[15] K. Aboudolas, M. Papageorgiou, A. Kouvelas, and E. Kosmatopoulos, "A rolling-horizon quadratic-programming approach to the signal control problem in large-scale congested urban road networks," *Transp. Res. C, Emerg. Technol.*, vol. 18, no. 5, pp. 680–694, Oct. 2010.

[16] R. Chen, D. Chen, and S. Lin, "ACTAM: Cooperative multi-agent system architecture for urban traffic signal control," *IEICE Trans. Inf. Syst.*, vol. 88, no. 1, pp. 119–126, 2005.

[17] S. Barman and M. W. Levin, "Throughput properties and optimal locations for limited deployment of max-pressure controls," *Transp. Res. C, Emerg. Technol.*, vol. 150, May 2023, Art. no. 104105.

[18] L. Li and S. E. Jabari, "Position weighted backpressure intersection control for urban networks," *Transp. Res. B, Methodol.*, vol. 128, pp. 435–461, Oct. 2019.

[19] T. Wongpiromsarn, T. Uthaicharoenpong, Y. Wang, E. Frazzoli, and D. Wang, "Distributed traffic signal control for maximum network throughput," in *Proc. 15th Int. IEEE Conf. Intell. Transp. Syst.*, Sep. 2012, pp. 588–595.

[20] P. Varaiya, "Max pressure control of a network of signalized intersections," *Transp. Res. C, Emerg. Technol.*, vol. 36, pp. 177–195, Nov. 2013.

[21] M. J. Smith and R. Mounce, "Backpressure or no backpressure? Two simple examples," *Transp. Res. C, Emerg. Technol.*, vol. 161, Apr. 2024, Art. no. 104515.

[22] M. W. Levin, J. Hu, and M. Odell, "Max-pressure signal control with cyclical phase structure," *Transp. Res. C, Emerg. Technol.*, vol. 120, Nov. 2020, Art. no. 102828.

[23] T. Le, P. Kovács, N. Walton, H. L. Vu, L. L. H. Andrew, and S. S. P. Hoogendoorn, "Decentralized signal control for urban road networks," *Transp. Res. C, Emerg. Technol.*, vol. 58, pp. 431–450, Sep. 2015.

[24] V. Dixit, D. J. Nair, S. Chand, and M. W. Levin, "A simple crowdsourced delay-based traffic signal control," *PLoS ONE*, vol. 15, no. 4, Apr. 2020, Art. no. e0230598.

[25] J. Wu, D. Ghosal, M. Zhang, and C.-N. Chuah, "Delay-based traffic signal control for throughput optimality and fairness at an isolated intersection," *IEEE Trans. Veh. Technol.*, vol. 67, no. 2, pp. 896–909, Feb. 2018.

[26] X. Wang, Y. Yin, Y. Feng, and H. X. Liu, "Learning the max pressure control for urban traffic networks considering the phase switching loss," *Transp. Res. C, Emerg. Technol.*, vol. 140, Jul. 2022, Art. no. 103670.

[27] M. W. Levin, D. Rey, and A. Schwartz, "Max-pressure control of dynamic lane reversal and autonomous intersection management," *Transportmetrica B, Transp. Dyn.*, vol. 7, no. 1, pp. 1693–1718, Dec. 2019.

[28] T. Xu, S. Barman, M. W. Levin, R. Chen, and T. Li, "Integrating public transit signal priority into max-pressure signal control: Methodology and simulation study on a downtown network," *Transp. Res. C, Emerg. Technol.*, vol. 138, May 2022, Art. no. 103614.

[29] D. Rey and M. W. Levin, "Blue phase: Optimal network traffic control for legacy and autonomous vehicles," *Transp. Res. B, Methodol.*, vol. 130, pp. 105–129, Dec. 2019.

[30] R. Chen, J. Hu, M. W. Levin, and D. Rey, "Stability-based analysis of autonomous intersection management with pedestrians," *Transp. Res. C, Emerg. Technol.*, vol. 114, pp. 463–483, May 2020.

[31] J. Lioris, A. Kurzhanskiy, and P. Varaiya, "Adaptive max pressure control of network of signalized intersections," *IFAC-PapersOnLine*, vol. 49, no. 22, pp. 19–24, 2016.

[32] J. Gregoire, E. Frazzoli, A. D. L. Fortelle, and T. Wongpiromsarn, "Back-pressure traffic signal control with unknown routing rates," *IFAC Proc. Volumes*, vol. 47, no. 3, pp. 11332–11337, 2014.

[33] T. Le, H. L. Vu, N. Walton, S. P. Hoogendoorn, P. Kovács, and R. N. Queija, "Utility optimization framework for a distributed traffic control of urban road networks," *Transp. Res. B, Methodol.*, vol. 105, pp. 539–558, Nov. 2017.

[34] A. A. Zaidi, B. Kulcsár, and H. Wymeersch, "Back-pressure traffic signal control with fixed and adaptive routing for urban vehicular networks," *IEEE Trans. Intell. Transp. Syst.*, vol. 17, no. 8, pp. 2134–2143, Aug. 2016.

[35] C. Liu, Z. Xu, Z. Liu, X. Li, and Y. Zhang, "Decentralized multi-vehicle motion planning for platoon forming in mixed traffic using Monte Carlo tree search," *IEEE Trans. Intell. Transp. Syst.*, vol. 25, no. 12, pp. 20872–20888, Dec. 2024.

[36] Y. Chen and Y. Liu, "Integrated optimization of planning and operations for shared autonomous electric vehicle systems," *Transp. Sci.*, vol. 57, no. 1, pp. 106–134, Jan. 2023.

[37] Z. Li et al., "Interaction dataset of autonomous vehicles with traffic lights and signs," *Commun. Transp. Res.*, vol. 5, Dec. 2025, Art. no. 100201.

[38] F.-Y. Wang et al., "Transportation 5.0: The DAO to safe, secure, and sustainable intelligent transportation systems," *IEEE Trans. Intell. Transp. Syst.*, vol. 24, no. 10, pp. 10262–10278, Oct. 2023.

[39] L. Li, V. Okoth, and S. E. Jabari, "Backpressure control with estimated queue lengths for urban network traffic," *IET Intell. Transp. Syst.*, vol. 15, no. 2, pp. 320–330, Feb. 2021.

[40] J. Gregoire, X. Qian, E. Frazzoli, A. de La Fortelle, and T. Wongpiromsarn, "Capacity-aware backpressure traffic signal control," *IEEE Trans. Control Netw. Syst.*, vol. 2, no. 2, pp. 164–173, Jun. 2015.
[41] P. Mercader, W. Uwayid, and J. Haddad, "Max-pressure traffic controller based on travel times: An experimental analysis," *Transp. Res. C, Emerg. Technol.*, vol. 110, pp. 275–290, Jan. 2020.
[42] C. V. Beojone and N. Geroliminis, "A dynamic multi-region MFD model for ride-sourcing with ridesplitting," *Transp. Res. B, Methodol.*, vol. 177, Nov. 2023, Art. no. 102821.
[43] D. Tsitsokas, A. Kouvelas, and N. Geroliminis, "Two-layer adaptive signal control framework for large-scale dynamically-congested networks: Combining efficient max pressure with perimeter control," *Transp. Res. C, Emerg. Technol.*, vol. 152, Jul. 2023, Art. no. 104128.
[44] Y. Xu, D. Li, and Y. Xi, "Perimeter traffic flow control for a multi-region large-scale traffic network with Markov decision process," *IEEE Trans. Intell. Transp. Syst.*, vol. 25, no. 6, pp. 4809–4821, Jun. 2024.
[45] S. Kumarage, M. Yildirimoglu, and Z. Zheng, "Demand and state estimation for perimeter control in large-scale urban networks," *Transp. Res. C, Emerg. Technol.*, vol. 153, Aug. 2023, Art. no. 104184.
[46] I. I. Sirmatel and N. Geroliminis, "Stabilization of city-scale road traffic networks via macroscopic fundamental diagram-based model predictive perimeter control," *Control Eng. Pract.*, vol. 109, Apr. 2021, Art. no. 104750.
[47] Z. C. Su, A. H. F. Chow, C. L. Fang, E. M. Liang, and R. X. Zhong, "Hierarchical control for stochastic network traffic with reinforcement learning," *Transp. Res. B, Methodol.*, vol. 167, pp. 196–216, Jan. 2023.
[48] H. Yu and M. J. Neely, "A new backpressure algorithm for joint rate control and routing with vanishing utility optimality gaps and finite queue lengths," *IEEE/ACM Trans. Netw.*, vol. 26, no. 4, pp. 1605–1618, Aug. 2018.
[49] M. J. Neely, "Energy optimal control for time varying wireless networks," *IEEE Trans. Inf. Theory*, vol. 52, no. 7, pp. 1–17, Aug. 2006.
[50] J. Liu, N. B. Shroff, C. H. Xia, and H. D. Sherali, "Joint congestion control and routing optimization: An efficient second-order distributed approach," *IEEE/ACM Trans. Netw.*, vol. 24, no. 3, pp. 1404–1420, Jun. 2016.
[51] S. Cui, Y. Xue, K. Gao, K. Wang, B. Yu, and X. Qu, "Delay-throughput tradeoffs for signalized networks with finite queue capacity," *Transp. Res. B, Methodol.*, vol. 180, Feb. 2024, Art. no. 102876.
[52] M. Treiber and A. Kesting, *Traffic Flow Dynamics: Data, Models and Simulation*. Berlin, Germany: Springer, 2013.
[53] K. Tiaprasert, Y. Zhang, X. B. Wang, and X. Zeng, "Queue length estimation using connected vehicle technology for adaptive signal control," *IEEE Trans. Intell. Transp. Syst.*, vol. 16, no. 4, pp. 2129–2140, Aug. 2015.
[54] Y. Mei, W. Gu, E. C. S. Chung, F. Li, and K. Tang, "A Bayesian approach for estimating vehicle queue lengths at signalized intersections using probe vehicle data," *Transp. Res. C, Emerg. Technol.*, vol. 109, pp. 233–249, Dec. 2019.
[55] D. Iwanowicz and K. Ostrowski, "Dilemmas of intersection queue length estimation in traffic capacity analyses," *Arch. Civil Eng.*, vol. 21, no. 1, pp. 523–541, Mar. 2025.
[56] J. Jithender and A. Mehar, "Estimation of queue length at signalized intersection under non-lane based traffic conditions," *Periodica Polytechnica Transp. Eng.*, vol. 51, no. 1, pp. 31–39, Nov. 2022.
[57] S. Cui, Y. Xue, K. Gao, M. Lv, and B. Yu, "Adaptive collision-free trajectory tracking control for string stable bidirectional platoons," *IEEE Trans. Intell. Transp. Syst.*, vol. 24, no. 11, pp. 12141–12153, Nov. 2023.

Shaohua Cui received the M.S. degree from the Systems Science Institute, School of Traffic and Transportation, Beijing Jiaotong University, in 2019, and the Ph.D. degree in transportation engineering from Beihang University in 2023. He is currently a Post-Doctoral Researcher with the Department of Architecture and Civil Engineering, Chalmers University of Technology (CTH). His research interests include traffic flow analysis, vehicle control, adaptive control, and robust control.

Lichao Wang received the M.S. degree in transportation engineering from Nanjing University of Aeronautics and Astronautics (NUAA), China, in 2020, and the Ph.D. degree in transportation engineering from Southeast University in 2024. He is currently an Associate Professor with the Civil Aviation University of China (CAUC). His research interests include connected autonomous vehicles, electric buses and platooning control, and low-altitude free flight.

Yongjie Xue is currently pursuing the Ph.D. degree with the School of Transportation Science and Engineering, Beihang University, China. His current research interests include traffic assignment, intelligent transportation systems, and big data for transportation.

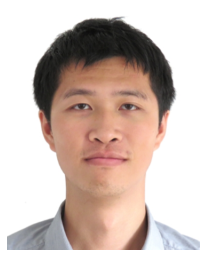

Kaidi Yang (Member, IEEE) received the B.Eng. and M.Sc. degrees from Tsinghua University, China, and the Ph.D. degree from ETH Zürich. He is currently an Assistant Professor with the Department of Civil and Environmental Engineering, National University of Singapore. Prior to this, he was a Post-Doctoral Researcher with the Autonomous Systems Laboratory, Stanford University. His main research interests include the operation of future mobility systems enabled by connected and automated vehicles (CAVs) and shared mobility.

Kun Gao (Member, IEEE) received the bachelor's and Ph.D. degrees from Tongji University. He is currently a Docent (Associate Professor) with the Department of Architecture and Civil Engineering, Chalmers University of Technology (CTH). The ultimate aim is to promote the sustainability of urban mobility by leveraging emerging transport technologies. His research interests include smart transport systems with focuses on electrification, shared mobility, and connected automation; machine learning and big data for transport studies; and travel behavior analysis. He has obtained research projects as a principal investigator in both Sweden and Europe in the above-mentioned areas. He has been publishing research outcomes in top-tier journals of transportation engineering and interdisciplinary areas.